AERODYNAMIC HEATING TO THE GAPS
AND SURFACES OF SIMULATED
REUSABLE-SURFACE-INSULATION
TILE ARRAYS IN TURBULENT
FLOW AT MACH 6.6

*Irving Weinstein, Don E. Avery,
and Andrew J. Chapman*

Langley Research Center
Hampton, Va. 23665

1. Report No. NASA TM X-3225	2. Government Accession No	3. Recipient's Catalog No.		
4. Title and Subtitle AERODYNAMIC HEATING TO THE GAPS AND SURFACES OF SIMULATED REUSABLE-SURFACE-INSULATION TILE ARRAYS IN TURBULENT FLOW AT MACH 6.6		5. Report Date November 1975		
		6. Performing Organization Code		
7. Author(s) Irving Weinstein, Don E. Avery, and Andrew J. Chapman		8. Performing Organization Report No. L-10188		
		10. Work Unit No. 506-17-22-01		
9. Performing Organization Name and Address NASA Langley Research Center Hampton, Va. 23665		11 Contract or Grant No.		
		13. Type of Report and Period Covered Technical Memorandum		
12. Sponsoring Agency Name and Address National Aeronautics and Space Administration Washington, D.C. 20546				
		14 Sponsoring Agency Code		

15. Supplementary Notes

16. Abstract

An experimental investigation was made on a simulated reusable-surface-insulation (RSI) tile array in a turbulent boundary layer to determine aerodynamic-heating distributions representative of those expected on the surface of the shuttle orbiter during Earth entry due to the presence of longitudinal and transverse surface gaps. The tests were conducted in the Langley 8-foot high-temperature structures tunnel in a test medium of methane-air combustion products at a nominal Mach number of 6.6 and over a free stream Reynolds number range from 2.0×10^6 to 4.9×10^6 per meter $(0.6 \times 10^6$ to 1.5×10^6 per foot). The results were used to assess the aerodynamic heating effects produced by parameters that include gap width, boundary-layer displacement thickness, in-line and staggered tile arrangement, and tile protrusion.

17. Key Words (Suggested by Author(s)) Gaps or cavities Space shuttle TPS Turbulent heat transfer	18 Distribution Statement Unclassifed – Unlimited Subject Category 34			
19. Security Classif (of this report) Unclassified	20 Security Classif. (of this page) Unclassified	21 No. of Pages 51	22 Price* $4.25	

AERODYNAMIC HEATING TO THE GAPS AND SURFACES

OF SIMULATED REUSABLE-SURFACE-INSULATION TILE ARRAYS

IN TURBULENT FLOW AT MACH 6.6

Irving Weinstein, Don E. Avery, and Andrew J. Chapman
Langley Research Center

SUMMARY

An experimental investigation was conducted on a thermal protection system (TPS) proposed for use on spacecraft. Simulated reusable-surface-insulation (RSI) tile arrays were tested to determine aerodynamic-heating distributions representative of those expected over the surface of the shuttle orbiter during Earth entry due to the presence of longitudinal and transverse surface gaps. The tests were conducted in the Langley 8-foot high-temperature structures tunnel at a nominal Mach number of 6.6 and a nominal total temperature of 1750 K (3150° R). The tests covered a free-stream Reynolds number range from 2.0×10^6 to 4.9×10^6 per meter $\left(0.6 \times 10^6 \text{ to } 1.5 \times 10^6 \text{ per foot}\right)$. The tiles were tested in both in-line and staggered arrangements and data were obtained for a relatively thin turbulent boundary layer over a range of gap widths from 0.10 to 0.41 cm (0.04 to 0.16 in.) and for boundary-layer displacement thicknesses from 0.81 to 1.62 cm (0.32 to 0.64 in.). Flat-plate tests were also made to provide comparison data.

The maximum heating rate to the in-line tile orientation was 1.8 times the local flat-plate value and occurred on top of the tile just behind the leading-edge radius. The heating to this arrangement was not appreciably affected by variations in either gap width or boundary-layer displacement thickness. The maximum heating to the staggered tile arrangement occurred on the forward face of the tile at the intersection of a longitudinal and a transverse gap and was as high as 2.9 times the flat-plate value. This impingement heating generally increased with an increase in gap width and with a decrease in boundary-layer displacement thickness. The most severe heating rate measured was 3.2 times the flat-plate value and occurred on the forward face of a tile that was raised approximately 20 percent of the boundary-layer displacement thickness above the surrounding tiles. The integrated heat flux to the vertical walls of an in-line tile arrangement was found to be over 40 percent higher than for the staggered tile arrangement. The total heat load to the entire tile was 13 percent higher for the in-line arrangement, indicating that the staggered tile arrangement could result in lower TPS mass.

INTRODUCTION

The space shuttle orbiter, which has a minimum design life of 100 missions, requires a reliable lightweight thermal protection system (TPS). (See ref. 1.) The current orbiter design uses a silica-based material for the reusable surface insulation (RSI) to isolate the primary structure from the extremely hostile aerodynamic environment. This material will be installed on the orbiter surface in the form of tiles which must be separated to allow for thermal expansion. The hot boundary-layer gases penetrate the gaps between the tiles and produce high local heating levels which may result in tile degradation or excessive structural temperatures. (See refs. 2 to 6.) The arrangement of the tiles relative to the flow and any vertical offset resulting from installation of the tiles may also influence the heating distributions over the surface. Current theories do not adequately predict the aerodynamic heating to the tile surfaces due to these gaps; consequently, the heating must be determined experimentally.

Wind-tunnel tests were made to determine the aerodynamic-heating-rate distributions to various simulated tile arrangements exposed to a turbulent boundary layer. The tests were made in the Langley 8-foot high-temperature structures tunnel at a nominal free-stream Mach number of 6.6, a nominal total temperature of 1750 K (3150° R), and free-stream Reynolds numbers from 2.0×10^6 to 4.9×10^6 per meter $\left(0.6 \times 10^6 \text{ to } 1.5 \times 10^6 \text{ per foot}\right)$. Cold-wall aerodynamic heating rates were obtained on a thin-wall metallic tile placed in the center of an RSI tile array. The tiles were approximately 6.4 cm (2.5 in.) deep by 15.2 cm (6.0 in.) square and the gap widths were varied from 0.10 cm (0.04 in.) to 0.41 cm (0.16 in.). The effects of gap width, boundary-layer displacement thickness, tile arrangement, and tile protrusion on the aerodynamic-heating distribution are presented herein.

SYMBOLS

Although physical quantities were measured in U.S. Customary Units, they are presented in this paper in the International System of Units (SI) also. Factors relating the two systems are given in reference 7.

c_p specific heat, J/kg-K (Btu/lb-°R)

dT/dt temperature rise rate, K/sec (°R/sec)

M   local Mach number

N   power-law exponent

2

N_{St}^* local Stanton number based on Eckert's reference temperature

$P_{t,c}$ combustor total pressure, Pa (psia)

q   cold-wall heating rate, W/m^2 (Btu/ft^2-sec)

q_{fp} flat-plate heating rate, W/m^2 (Btu/ft^2-sec)

R^* local Reynolds number based on Eckert's reference temperature

R_∞ free-stream Reynolds number per meter (per foot)

r   tile edge radius, cm (in.)

s   peripheral distance along tile sidewall, cm (in.)

T   temperature, K (^{O}R)

T_t tunnel total temperature, K (^{O}R)

t   time, sec

U   velocity, m/sec (ft/sec)

U_o velocity at edge of boundary layer, m/sec (ft/sec)

w   gap width, cm (in.)

x,y,z   model coordinates (see fig. 5), cm (in.)

$\bar{y}$ coordinate of boundary-layer profile (measured normal to surface, fig. 10), cm (in.)

α angle of attack, deg

δ boundary-layer thickness, cm (in.)

δ^* boundary-layer displacement thickness, cm (in.)

ρ material density, kg/m^3 (lb/ft^3)

τ wall thickness, cm   (in.)

MODELS AND TEST APPARATUS

RSI Tile Array

The tile array consisted of 10 RSI tiles (material is designated as LI-942) surrounding a metallic center tile as shown schematically in figure 1. All heating-rate data were obtained with the metallic tile, and the RSI tiles were used to complete the simulated array. The tile array was approximately 46 cm (18 in.) square. Individual tile dimensions are given in the table in figure 1. All tiles had a total thickness of 6.50 cm (2.56 in.), which also gave a gap depth of 6.50 cm (2.56 in.). The tiles were all attached to a common support plate to form the simulated array. Slotted holes in the support plate allowed each tile to be adjusted to vary the gap width between tiles. The center tile, made of 304 stainless steel, was 15.2 cm (6.0 in.) square and had a wall thickness of 0.051 cm (0.020 in.). All tiles had a nominal edge radius of 0.25 cm (0.10 in.). The tile arrangement was changed by rotating the RSI (or surrounding) tile array 90°. The thin-wall metallic tile was maintained with the same orientation to the flow for all tests to keep a consistency of the measurement location and a repeatability of the data. For the raise tile tests, a shim was placed under the center tile to raise it 0.25 cm (0.10 in.) above the level of the surrounding tiles.

Calibration Panel

The calibration panel, which is shown in figure 2, consisted of a 0.051-cm (0.020-in.) thick 304 stainless-steel plate 46 cm (18 in.) wide by 48 cm (19 in.) long. This plate was supported by a 1.27-cm (0.5-in.) thick "marinite" fiberboard grid spaced at 3.6 cm (1.4 in.) intervals in the longitudinal direction and 13.0 cm (5.1 in.) in the transverse direction to provide structural stiffness and minimize the chance of buckling due to pressure loads during testing. The overall panel depth was about 10 cm (4 in.). The calibration panel was used to obtain heating rates to a smooth flat surface for comparison with data obtained on the surface of the tile array.

Panel Holder

The panel-holder configuration used for these tests is shown in figure 3. The panel holder is a rectangular slab which has a sharp wedge-shaped leading edge. Panels as large as 108 by 152 cm (42.5 by 60 in.) can be tested in this holder. The surface surrounding the test panel is covered with 2.5-cm (1-in.) thick low-conductivity silica tiles.

Boundary-layer trips and aerodynamic fences are used to produce uniform two-dimensional flow over the entire surface. More details of the panel holder and the flow conditions over the surface are presented in reference 8. The tile array was centered approximately 213 cm (84 in.) aft of the panel-holder leading edge as shown in figure 3. A photograph of the calibration panel in the panel holder in the Langley 8-foot high-temperature structures tunnel is shown in figure 4.

Instrumentation

The metallic tile was instrumented with 92 No. 30 gage chromel-alumel thermocouples with the wires spotwelded to the inside surface at the locations shown in the schematic drawing in figure 5. The thermocouple locations along the center line near the leading edge are shown in the enlargement in the figure. The coordinate system used for the data plots is shown in the figure with the origin for this system located at the center of the tile.

The thermocouple locations on the calibration panel are shown in figure 6. Thirty-five No. 30 gage chromel-alumel thermocouples were spotwelded to the inside surface of the panel. The thermocouples were spaced 6.4 cm (2.5 in.) apart longitudinally and 8.9 cm (3.5 in.) apart laterally.

Data obtained on the panel holder included measurements of the surface and base pressures and the cavity temperature and pressures at the locations indicated in figure 3. A key identifying the type of measurement is given in the figure. Static and pitot pressures in the boundary layer were also measured using a traversing boundary-layer rake located just forward of the test panel. A photograph of the survey rake in the extended position is shown in figure 7. The pitot pressure orifice had an outside diameter of 0.15 cm (0.06 in.) and an inside diameter of 0.10 cm (0.04 in.).

Test Facility

The tests were conducted in the Langley 8-foot high-temperature structures tunnel which is shown schematically in figure 8. This facility is a hypersonic blowdown tunnel which has a high energy level that is obtained by burning a mixture of methane and air under high pressure. The products of combustion are then expanded through an axisymmetric contoured nozzle to a nominal Mach number of 7 and into the open jet test section to obtain hypersonic flight simulation. The flow goes into a supersonic diffuser where it is pumped through a mixing tube and exhausted to the atmosphere by means of a single-stage annular air ejector. This tunnel can be operated at total temperatures between 1400 and 2000 K (2500° and 3600° R) and at combustor total pressures from 4.1 to 24.1 MPa (600 to 3500 psia). The corresponding free-stream Reynolds numbers are between 1×10^6 and 10×10^6 per meter $\left(0.3 \times 10^6 \text{ and } 3.0 \times 10^6 \text{ per foot}\right)$. These conditions simulate the

hypersonic flight environment in the altitude range between 25 and 40 km (80 000 and 130 000 ft).

The models are mounted on an elevator and inserted into the stream after the test conditions are established to avoid tunnel transients which occur during tunnel start up and shut down. A model pitch system provides an angle-of-attack range of ±20°. More detailed information can be found in reference 8 and a description and list of operating conditions are reported in references 9 and 10.

TEST PROCEDURE AND DATA REDUCTION

The model was located in the pod below the test region as shown schematically in figure 8. After the tunnel equilibrium flow conditions were established, the model was inserted rapidly into the test stream while simultaneously being pitched to the desired angle of attack to give as nearly as possible a step-function exposure to the test environment. The model angle of attack, the model position, and a typical temperature on the metallic tile are shown as a function of time in figure 9 to illustrate the sequence of events which occurs as the model is inserted into the test stream. The model reaches the desired angle of attack before reaching the tunnel center line. The time of data analysis, which was taken as the time when the panel holder reached the tunnel center line, is indicated in the figure.

The thermocouple and pressure transducer outputs were recorded on the Langley central data recording system at a rate of 20 samples per second and converted to temperatures and pressures. Cold-wall heating rates were obtained using temperature data over a 3-sec interval. A fourth-order polynomial was fit to the temperature history in this time interval starting approximately 1 sec before the model reached the tunnel center line. The slope of the polynomial at the time the model reached the tunnel center line was used in the one-dimensional transient heat balance equation, $q = \rho c_p \tau dT/dt$. This equation equates the convective energy entering the surface to the energy stored, and does not consider the effects of conduction and radiation. These assumptions are considered reasonable since the temperature-time slopes were taken early in the tests when the surface temperatures were relatively low.

The test conditions for ⸱ ch tile arrangement and the calibration panel are given in table I. Three runs were made on the calibration panel and 16 runs were made on the tile array configurations. The tests were made at tunnel total temperatures from 1530 to 1890 K (2760° to 3400° R) and the free-stream Reynolds number varied from about 2.0×10^6 to 4.9×10^6 per meter $\left(0.6 \times 10^6 \text{ to } 1.5 \times 10^6 \text{ per foot}\right)$. The free-stream test conditions were determined from temperatures and pressures measured in the combustor and are based on the thermal, transport, and flow properties of methane-air combustion products as reported in reference 11 and the tunnel surveys of reference 8.

6

RESULTS AND DISCUSSION

Boundary-Layer Surveys

A boundary-layer survey probe was used to obtain boundary-layer pitot and static pressure measurements for several different tunnel conditions. The pitot and static boundary-layer pressure distributions obtained during run 10 (table I) are shown in figure 10. The pressures are plotted for distances measured normal from the model surface to the location of the center of the orifice. The intersection of the linear and constant-pressure portion of the pitot pressure distribution was used to define the boundary-layer thickness. A jump in the pitot pressure level, which was characteristic of all the distributions obtained, occurs in the region near the edge of the boundary layer. This change in pressure level may have been influenced by pressure wave interference.

A boundary-layer velocity profile was obtained by determining the local Mach number from the measured pitot and static pressures with the use of the standard Rayleigh pitot equations and with the assumption of constant static pressure and total temperature across the boundary layer. (See ref. 12.) The boundary-layer velocity profile obtained by this procedure using the pressure distributions of figure 10 is presented in figure 11. The shape of this profile is characteristic of that for turbulent boundary layers as indicated by a 1/12.5 power-law curve fit to the data. An experimental value of the boundary-layer displacement thickness was obtained by integrating the velocity profile. Theoretical values of the boundary-layer thickness and the boundary-layer displacement thickness were obtained with the use of the computer program described in reference 13. Comparisons of the experimental and theoretical boundary-layer thicknesses at the boundary-layer probe location of 180 cm (71 in.) from the panel-holder leading edge are presented in table II for three test conditions. The experimental values of both δ and δ^* are higher than the calculated values but the agreement between the experimental and calculated values is within 10 percent. The boundary-layer displacement thickness used in the presentation of the data is the theoretical value obtained 2.13 m (7.0 ft) aft of the panel-holder leading edge, which is at the center of the instrumented metallic tile.

Flat-Plate Heating Distributions

Three test runs were made on the calibration panel to obtain flat-plate cold-wall heating rates for comparison with those obtained on the tile arrays. The longitudinal and transverse heating distributions for run 1 are presented in figures 12(a) and 12(b), respectively. Although the heating varied near the edges of the panel, the distributions over the center 20 cm (8 in.) which covers the area filled by the metallic center tile of the test model, are uniform within ±3 percent.

The heating rates obtained along the longitudinal center line of the calibration panel near the leading edge, at the center, and near the trailing edge for the three runs are presented in the form of a local cold-wall Stanton number in figure 13 as a function of the local Reynolds number. The curves in the figure are for laminar and turbulent heating obtained from the relationships given in reference 14. The Stanton and Reynolds numbers are based on properties evaluated at Eckert's reference temperature as described in reference 15. The data shown represent the lower range of local Reynolds number for all the heat-transfer tests and are in good agreement with the turbulent-theory curve. Consequently, it is assumed that all tests conducted had a turbulent boundary layer.

In-Line Tile Arrangement

Of the 16 runs made on the tile array, 6 runs were made on an in-line arrangement where the tiles are alined in the flow direction resulting in continuous longitudinal gaps. (See fig. 1.) The tests were made at nominal values of the gap width and the boundary-layer displacement thickness as given in table III. Heating rates obtained at the center of the metallic tile were generally within 5 percent of those at the center of the calibration panel, after accounting for variation in test conditions. Since it was difficult to repeat test conditions from run to run, the heating rate obtained at the center of the metallic tile was taken as the equivalent flat-plate heating rate and the heating data are presented as a nondimensional function of this value. The value of the equivalent flat-plate heating rate for each run is given in table III.

Typical heating-rate distributions.- Typical nondimensional heating-rate distributions over the top surface and vertical faces of the metallic center tile are presented in figure 14 for the in-line tile arrangement. (See fig. 1.) The data are shown for run 6 which had a gap width of 0.18 cm (0.07 in.) and a boundary-layer displacement thickness of 1.17 cm (0.46 in.).

The longitudinal distributions on the forward face, along the top, and down the back face of the tile are shown in figure 14(a) for three transverse locations. The tick marks on the tile profile above the data indicate the thermocouple locations relative to the data plot. The heating is very low near the bottom of the gap but increases rapidly near the top of the forward face and reaches a maximum on the top surface just aft of the leading-edge radius. The maximum measured heating for this condition was 1.8 times the flat-plate value. The heating then decreases and levels off to near the flat-plate value. The heating decreases further near the trailing edge of the surface and then drops off abruptly down the back face of the tile. The longitudinal distributions on the top surface are cross plotted at three transverse locations in figure 14(b). The maximum measured heating rate to all in-line arrangements tested consistently occurred on top of the tile just behind the leading-edge radius.

8

The heating along the vertical faces of the tile is presented in figure 14(c) for three depths into the gaps. The sketch at the top of the figure is a foldout of the sides of the tile relating the measurement locations to the plotted distributions. The heating is low along the forward face except near the corner and close to the top surface where the longitudinal gap flow spills into the transverse gap resulting in heating 20 percent higher than the flat-plate value. The heating is fairly constant along the sidewall due to the development of flow occurring in a continuous longitudinal gap and the heating level approaches that of the flat-plate value near the top of the sidewall and decreases rapidly with depth into the gap.

Effect of gap width on heating.- The nondimensional heating-rate distributions along the longitudinal center line of the tile are shown in figure 15(a) for three gap widths and a boundary-layer displacement thickness of 1.17 cm (0.46 in.). The figure shows a similar trend of heating for all gap widths with the peak heating occurring downstream from the leading-edge radius. The effect of the gap width on the heating for locations near the leading edge of the tile is shown in figure 15(b). It can be seen that the maximum heating occurs on the top surface just behind the leading-edge radius (location 3) and increases slightly with an increase in the transverse gap width.

The center-line heating distributions on the forward and rear tile walls for the same three gap widths are presented in figure 15(c) to an expanded scale. The heating reduces very rapidly with depth into the gap for all gap widths. The heating is lowest on both the forward and rear walls for a gap width of 0.18 cm (0.07 in.) and then shows a large increase when the gap width is increased.

Effect of boundary-layer displacement thickness on heating.- The nondimensional heating-rate distributions along the tile longitudinal center line for three values of the boundary-layer displacement thickness and for a gap width of 0.18 cm (0.07 in.) are presented in figure 16(a). The maximum heating occurs behind the leading edge for each value of the displacement thickness. The effect of the displacement thickness on the maximum heating is shown in figure 16(b). The heating for the locations in or near the tile leading-edge radius decreases with an increase in displacement thickness; however, at a location farther back on the top surface the heating increases slightly with an increase in displacement thickness. The maximum heating occurs on the top surface just aft of the leading-edge radius except for the largest displacement thickness, where the maximum heating occurred 3.8 cm (1.5 in.) aft of the leading edge.

The center-line heating distributions on the forward and rear walls for three values of the boundary-layer displacement thickness are shown in figure 16(c) on an expanded scale. The heating increases on both faces as the displacement thickness is decreased.

9

Staggered Tile Arrangement

For the staggered tile arrangement (see fig. 1), a highly localized heating region occurs where the longitudinal gap terminates and the flow impinges on a forward facing wall. (See ref. 2.) For accurate measurements of the peak heating in this region the thermocouples must be in good alinement with the longitudinal gap. Due to some inconsistencies in the heating results, measurements of the thermocouple spotweld locations were made. It was found that the center row of thermocouples on the forward face of the tile in the impingement region was misalined as much as 0.046 cm (0.18 in.) from the gap center line. This misalinement, which varied from 20 to 90 percent of the gap half-width, may have resulted in measurements of heating that were lower than the values existing at the gap center line.

Typical heating-rate distributions.- Typical nondimensionalized heating-rate distributions for the staggered tile arrangement are presented in figure 17. The data presented are for a gap width of 0.18 cm (0.07 in.) and a boundary-layer displacement thickness of 1.17 cm (0.46 in.). The longitudinal heating-rate distributions at three lateral locations are given in figure 17(a). As indicated in the figure, high heating occurs on the forward face of the tile in the flow-impingement region at the end of the longitudinal gap. The heating is much higher down the entire wall in this region than for other lateral locations. For these test conditions the peak heating was about 2.6 times the flat-plate value. A sharp but less severe peak in the heating also occurred on the downstream wall of the tile near the corner. The latter increase in heating is probably caused by the flow in the longitudinal side gap impinging on the next tile and spilling into the transverse gap behind the tile. The transverse heating-rate distributions are shown in figure 17(b) for locations near the leading edge, at the lateral center line, and near the trailing edge of the tile. These transverse distributions differ from those shown in figure 14(b) for an in-line arrangement primarily near the leading edge where the staggered arrangement has high heating near the center line due to flow impingement but blocks the flow near the corner and results in lower heating.

The heating distributions around the perimeter at three depths into the gap are shown in figure 17(c). The heating at 0.5 cm (0.2 in.) into the gaps is more than twice the flat-plate value at the center of the forward face and then decreases abruptly to the edge of the tile. The heating level then increases gradually along the side to about 0.6 times the flat-plate value near the corner. The heating more than doubles on the rear wall near the corner as a result of the flow spillage into the transverse gap behind the tile. The heating rate decreases with additional distance along the rear wall. This heating-rate distribution is significantly different from that shown in figure 14(c) for the in-line tile arrangement. Although there are no large heating peaks for the in-line arrangement, the heating level on the sidewall is approximately constant but higher than for the staggered arrangement.

10

This variation in the sidewall heating distribution may be attributed to limiting the development of flow in the longitudinal gap to one tile length for the staggered tiles, whereas the longitudinal gap is continuous for the in-line tiles.

A comparison of the integrated heat flux to the vertical walls of these two tile arrangements indicated that the vertical-wall heat load is over 40 percent higher for the in-line arrangement. The total heat load to the entire tile w s 13 percent higher for the in-line tile arrangement. This heating indicates that the staggered arrangement could result in lower TPS mass and may be preferred over the in-line arrangement, but only if tile integrity in the impingement region is maintained.

Effect of gap width on heating.- The nondimensional heating-rate distributions along the longitudinal center line are presented in figure 18(a) for several gap widths and a boundary-layer displacement thickness of 1.17 cm (0.46 in.). The data show a very sharp rise in the heating in the impingement region near the top of the tile. The heating in the impingement region is shown in figure 18(b) for the three locations indicated in the sketch in the figure. The maximum heating occurs in the leading-edge radius along the tile center line for all gap widths tested. The heating increases with an increase in gap width up to 0.30 cm (0.12 in.) where the heating is a maximum of approximately 2.9 times the flat-plate value. These heating values shown may be somewhat affected by the offset of the thermocouples relative to the gap center line.

The heating distributions down the forward and rear tile walls along the tile center line are shown in figure 18(c). The heating is very high on the forward wall and decreases gradually into the gap. The heating level increases for the larger gap widths. A comparison of this heating wi' that for the in-line arrangement shown in figure 15(c) shows the extreme effect of flow impingement on the local heating levels. The nondimensional heating rates are low and show little variation down the rear wall of the tile.

Effect of boundary-layer displacement thickness on heating.- The heating distributions along the tile center line are shown in figure 19(a) for three values of the boundary-layer displacement thickness for a gap width of 0.18 cm (0.07 in). The heating in the impingement region is shown in figure 19(b) over the range of displacement thickness tested. The heating is highest for a displacement thickness of 1.17 cm (0.46 in.) and then decreases with an increase in displacement thickness. The maximum heating occurs in the corner radius except for the largest displacement thickness of 1.62 cm (0.64 in.) where the maximum heating is on the top surface just behind the tile leading edge.

The heating distributions on the forward and rear walls along the center line are shown in figure 19(c). The heating on the forward wall is low for the largest displacement thickness but the heating is high for all other values of the displacement thickness. The heating down the rear wall is low for all values of displacement thickness.

Heating Effect of Raised Tile

In-line tile arrangement.- The nondimensional heating distributions along the tile center line for a raised- and a flush-tile array are presented in figure 20 for the in-line tile arrangement. The data presented are for a tile raised 0.25 cm (0.10 in.) above the flush surface, for a displacement thickness of 1.17 cm (0.46 in.), and for a gap width of 0.18 cm (0.07 in.). The maximum heating rate along the center line was 3.2 times the flat-plate value and more than twice the flush-tile value.

The heating on the forward face for the raised and flush tiles is shown in figure 20(b). The heating rates for the raised tile are much higher over the entire forward face than for the flush tile; consequently, the raised tile could cause an increase in the substructure temperature.

Staggered tile arrangement.- A comparison of the nondimensionalized heating along the center line for a raised and a flush tile in the staggered tile arrangement is presented in figure 21. Data are presented for a boundary-layer displacement thickness of 1.17 cm (0.46 in.) and a gap width of 0.18 cm (0.07 in.). The maximum heating rate is about three times the flat-plate value and about 15 percent higher than impingement heating for the flush tile. The heating distributions on the forward face along the center line for a staggered tile arrangement are shown in figure 21(b). The heating down the forward face at the tile center line is approximately the same for both a raised and a flush tile. The maximum heating level is approximately the same for a raised tile in both the staggered and the in-line arrangement.

CONCLUDING REMARKS

Heat transfer rates were obtained from temperatures measured on the surfaces of a simulated reusable-surface-insulation tile array in a turbulent boundary layer in the Langley 8-foot high-temperature structures tunnel. The tile array was approximately 46 cm (18 in.) square and consisted of individual tiles about 15 cm (6 in.) square. The tests were made in a test medium of methane-air combustion products at a nominal Mach number of 6.6 and a nominal total temperature of 1750 K (3150° R). The tests covered a free-stream Reynolds number range from 2.0×10^6 to 4.9×10^6 per meter $\left(0.6 \times 10^6 \text{ to } 1.5 \times 10^6 \text{ per foot}\right)$. Cold-wall aerodynamic heating rates were obtained on a thin-wall metallic tile placed in the center of the RSI tile array to assess the effects of gap width, boundary-layer displacement thickness, tile arrangement, and tile protrusion on the heating distributions.

The results indicated that the maximum heating rate to an in-line tile arrangement occurred at the largest gap width and was 1.8 times the local flat-plate value. The

maximum heating for this tile arrangement consistently occurred on top of the tile just behind the leading-edge radius. The heating along the center line for this arrangement was only mildly affected by variations in both gap width and boundary-layer displacement thickness.

The maximum heating rate to a staggered tile arrangement was approximately 2.9 times the local flat-plate value and occurred consistently on the leading-edge radius along the tile center line, which was in the flow-impingement region at the end of a longitudinal gap. This impingement heating generally increased with an increase in gap width and with a decrease in boundary-layer displacement thickness.

The most severe heating rate measured was 3.2 times the flat-plate value and occurred on a tile that was raised approximately 20 percent of the boundary-layer displacement thickness above the surrounding tiles. The tile arrangement (in-line or staggered) had very little effect on the maximum heating to a raised tile.

The integrated heat flux to the vertical walls of an in-line tile arrangement was found to be over 40 percent higher than that for the staggered tile arrangement. The total heat load to the entire tile was 13 percent higher for the in-line tile arrangement. This heating indicates that the staggered tile arrangement could result in lower mass of the thermal protection system and may be preferred over the in-line arrangement, but only if tile integrity in the impingement region for the staggered tile arrangement is maintained.

Langley Research Center
National Aeronautics and Space Administration
Hampton, Va. 23665
August 14, 1975

REFERENCES

1. Anderson, Roger A.; Brooks, William A., Jr.; Leonard, Robert W.; and Maltz, Joseph: Structures — A Technology Overview. Astronaut. & Aeronaut., vol. 9, no. 2, Feb. 1971, pp. 38-47.

2. Hunt, L. Roane; and Bohon, Herman L.: Performance of LI-1542 Reusable Surface Insulation System in a Hypersonic Stream. NASA TM X-71955, 1974.

3. Johnson, Charles B.: Heat Transfer Data to Cavities Between Simulated RSI Tiles at Mach 8. NASA CR-128770, 1973.

4. Throckmorton, David A.: Heat Transfer to Surface and Gaps of RSI Tile Arrays in Turbulent Flow at Mach 10.3. NASA TM X-71945, 1974.

5. Dunavant, James C.; and Throckmorton, David A.: Aerodynamic Heat Transfer to RSI Tile Surfaces and Gap Intersections. J. Spacecraft & Rockets, vol. 11, no. 6, June 1974, pp. 437-440.

6. Bohon, Herman L.; Sawyer, J. Wayne; Hunt, L. Roane; and Weinstein, Irving: Performance of Full Size Metallic and RSI Thermal Protection Systems in a Mach 7 Environment. AIAA Paper No. 75-800, May 1975.

7. Metric Practice Guide. E 380-72, American Soc. Testing & Mater., June 1972.

8. Deveikis, William D.; and Hunt, L. Roane: Loading and Heating of a Large Flat Plate at Mach 7 in the Langley 8-Foot High-Temperature Structures Tunnel. NASA TN D-7275, 1973.

9. Schaefer, William T., Jr.: Characteristics of Major Active Wind Tunnels at the Langley Research Center. NASA TM X-1130, 1965.

10. Pirrello, C. J.; Hardin, R. D.; Heckart, M. V.; and Brown, K. R.: An Inventory of Aeronautical Ground Research Facilities. Vol. I — Wind Tunnels. NASA CR-1874, 1971.

11. Leyhe, E. W.; and Howell, R. R.: Calculation Procedure for Thermodynamic, Transport, and Flow Properties of the Combustion Products of a Hydrocarbon Fuel Mixture Burned in Air With Results for Ethylene-Air and Methane-Air Mixtures. NASA TN D-914, 1962.

12. Heller, Hanno H.; and Holmes, D. Graham: Unsteady Aerodynamic Loads During Reentry of the Straight-Wing Orbiter Configuration. NASA CR-111960, 1971.

13. Anderson, E. C.; and Lewis, C. H.: Laminar or Turbulent Boundary-Layer Flows of Perfect Gases or Reacting Gas Mixtures in Chemical Equilibrium. NASA CR-1893, 1971.

14. Kays, W. M.: Convective Heat and Mass Transfer. McGraw-Hill Book Co., Inc., c.1966.

15. Eckert, Ernst R. G.: Survey on Heat Transfer at High Speeds. ARL 189, U.S. Air Force, Dec. 1961.

TABLE I.- TEST CONDITIONS FOR GAP HEATING TESTS

Run.	T_t		$p_{t,c}$		R_∞		M	α, deg	Test configuration
	K	^{o}R	MPa	psia	per meter	per foot			
1	1690	3050	7.10	1030	1.97×10^6	0.60×10^6	5.26	7.7	Calibration panel
2	1720	3100	6.55	950	1.87	.57	6.41	.1	
3	1720	3100	17.86	2590	4.69	1.43	6.25	.1	
4	1710	3070	7.17	1040	2.00	.61	5.26	7.6	In-line tile
5	1710	3070	7.21	1045	2.00	.61	5.26	7.5	
6	1770	3190	7.17	1040	1.97	.60	5.26	7.7	
7	1840	3320	7.03	1020	1.90	.58	6.90	-.1	
8	1720	3100	7.14	1035	2.00	.61	4.22	15.0	
9	1890	3400	7.14	1035	1.87	.57	5.56	7.6	
10	1530	2760	7.10	1030	2.07	.63	5.26	7.3	Staggered tile
11	1660	2980	7.17	1040	2.00	.61	6.45	-.1	
12	1700	3060	7.21	1045	2.00	.61	4.17	15.1	
13	1830	3300	7.21	1045	1.97	.00	5.56	7.6	
14	1640	2950	7.38	1070	2.10	.64	5.26	7.4	
15	1670	3000	7.17	1040	2.00	.61	5.32	7.5	
16	1770	3180	7.27	1055	2.03	.62	5.35	7.5	
17	1730	3120	18.06	2620	4.82	1.47	5.26	7.6	
18	1820	3280	17.93	2600	4.69	1.43	6.45	-.1	
19	1830	3300	18.06	2620	4.69	1.43	6.45	.1	

TABLE II.- COMPARISONS OF EXPERIMENTAL AND THEORETICAL
BOUNDARY-LAYER VALUES 180 cm   (71 in.)   FROM
LEADING EDGE OF PANEL HOLDER

T_t		$P_{t,c}$		$\alpha,$ deg	δ_{exp}		δ_{theor}		δ^*_{exp}		δ^*_{theor}	
K	°R	MPa	psia		cm	in.	cm	in.	cm	in.	cm	in.
1533	2760	7.1	1030	7.3	2.69	1.06	2.41	0.95	1.07	0.42	1.02	0.40
1900	3420	7.0	1015	14.9	2.39	.94	2.18	.86	.79	.31	.71	.28
1717	3090	17.9	2600	7.4	2.26	.89	2.13	.84	.81	.32	.81	.32

TABLE III.- MODEL TEST VARIABLES

Run	Test configuration	Nominal gap width		Step height		Nominal δ*		q_{fp}	
		cm	in.	cm	in.	cm	in.	kW/m²	Btu/ft²-sec
1	Calibration panel	---	---	---	---	1.17	0.46	74.4	6.56
2	↓	---	---	---	---	1.62	.64	36.1	3.18
3		---	---	---	---	1.38	.54	63.6	5.60
4	In-line tile	0.41	0.16	0.0	0.0	1.17	.46	77.1	6.79
5		.30	.12			↓	↓	72.6	6.40
6		.18	.07			↓	↓	75.7	6.67
7						1.62	.64	43.0	3.79
8				↓	↓	.81	.32	125.6	11.07
9	↓			.25	.10	1.17	.46	81.8	7.21
10	Staggered tile			.0	.0	1.17	.46	65.4	5.76
11						1.62	.64	35.7	3.15
12		↓	↓			.81	.32	125.3	11.04
13		.10	.04			1.17	.46	76.7	6.76
14		.30	.12			↓	↓	70.9	6.25
15		.41	.16	↓	↓			72.0	6.34
16		.18	.07	.25	.10	↓	↓	80.0	7.05
17		↓	↓	.0	.0	.96	.38	136.5	12.03
18		↓	↓			1.38	.54	61.6	5.43
19	↓	.41	.16	↓	↓	1.38	.54	73.1	6.44

Tile no. (See sketch)	Tile sizes	
	cm	in.
1	15.24 × 15.24	6.0 × 6.0
2	13.72 × 14.48	5.4 × 5.7
3	15.24 × 13.72	6.0 × 5.4
4	13.72 × 7.24	5.4 × 2.85

Flow direction for in-line tile arrangement

46 (18)

46 (18)

Flow direction for staggered tile arrangement

0.051 (0.020) 304 S.S.   center tile

Complete RSI tile system

Support plate

Section A-A

6.50 (2.56)
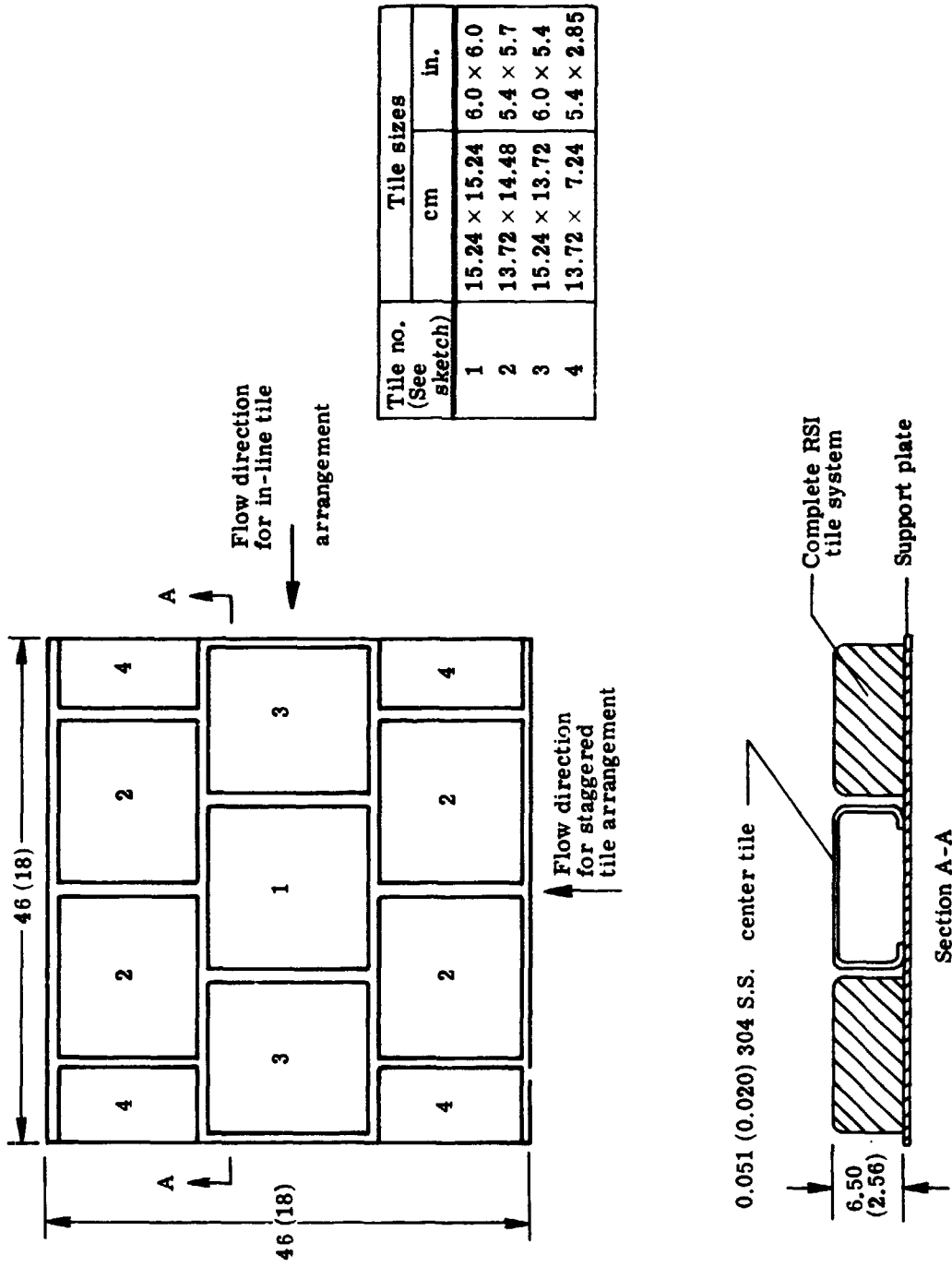
Figure 1.- Schematic drawing of tile layout and details of test model. Dimensions are in cm (in.).
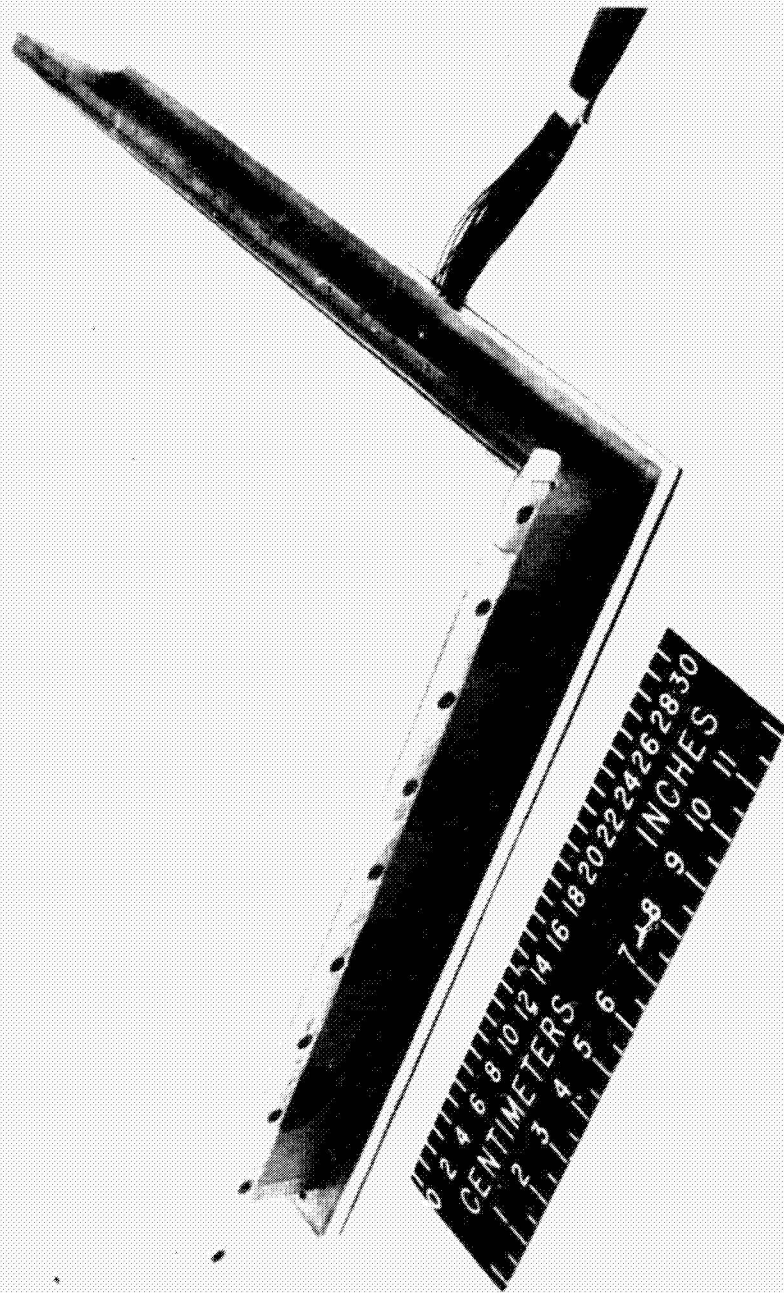
Figure 2.- Photograph of calibration panel.

L-74-5059

142
(56)

108
(42.5)

152 (60)

15
(6)

48
(19)

46
(18)

213 (84)

102 (40)

13 (5)

Flow

Flow trips

● Thermocouple
○ Pressure orifice
⊖ Boundary layer rake

Aerodynamic fences
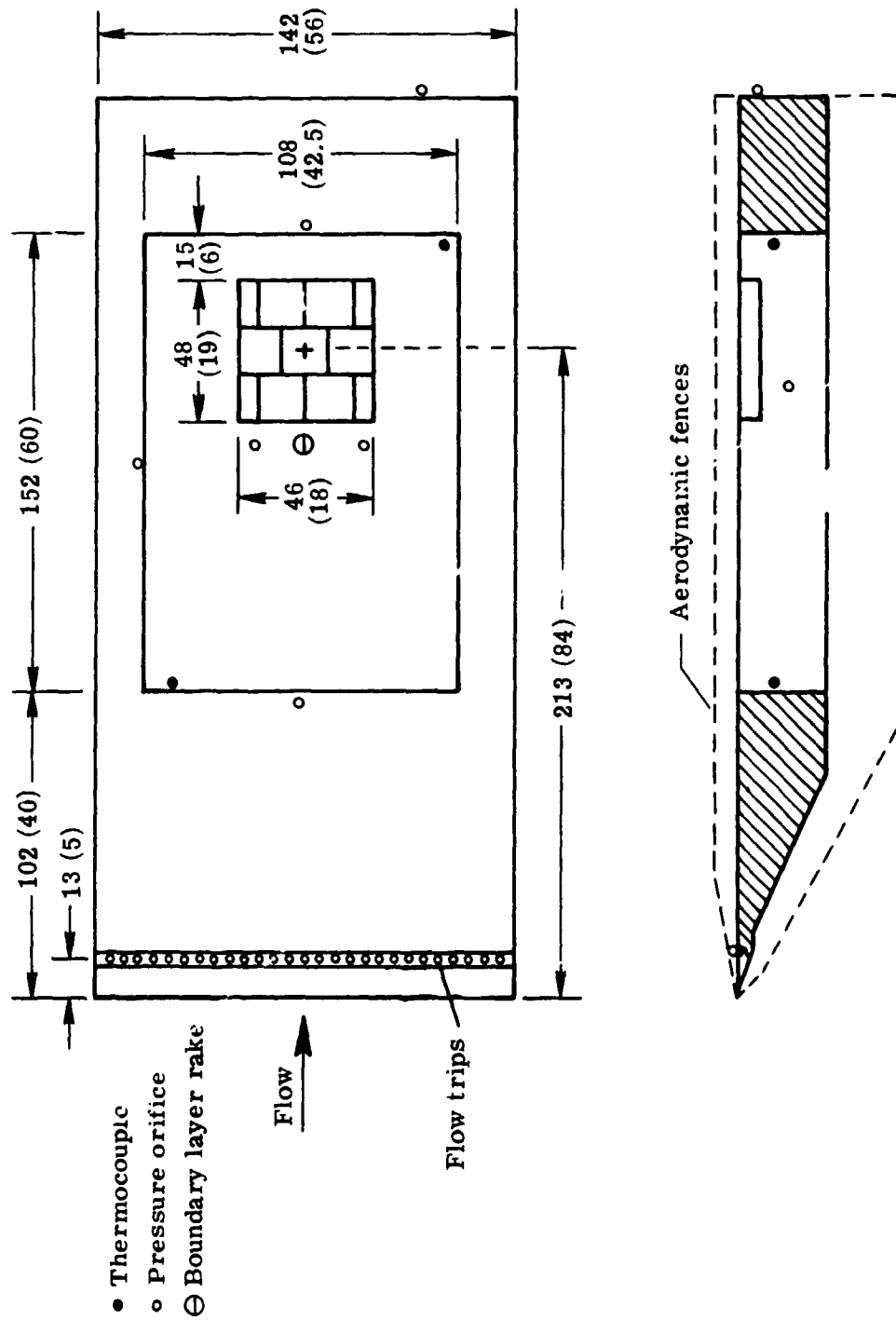
Figure 3.- Panel-holder details and instrumentation.
Dimensions are in cm (in.).
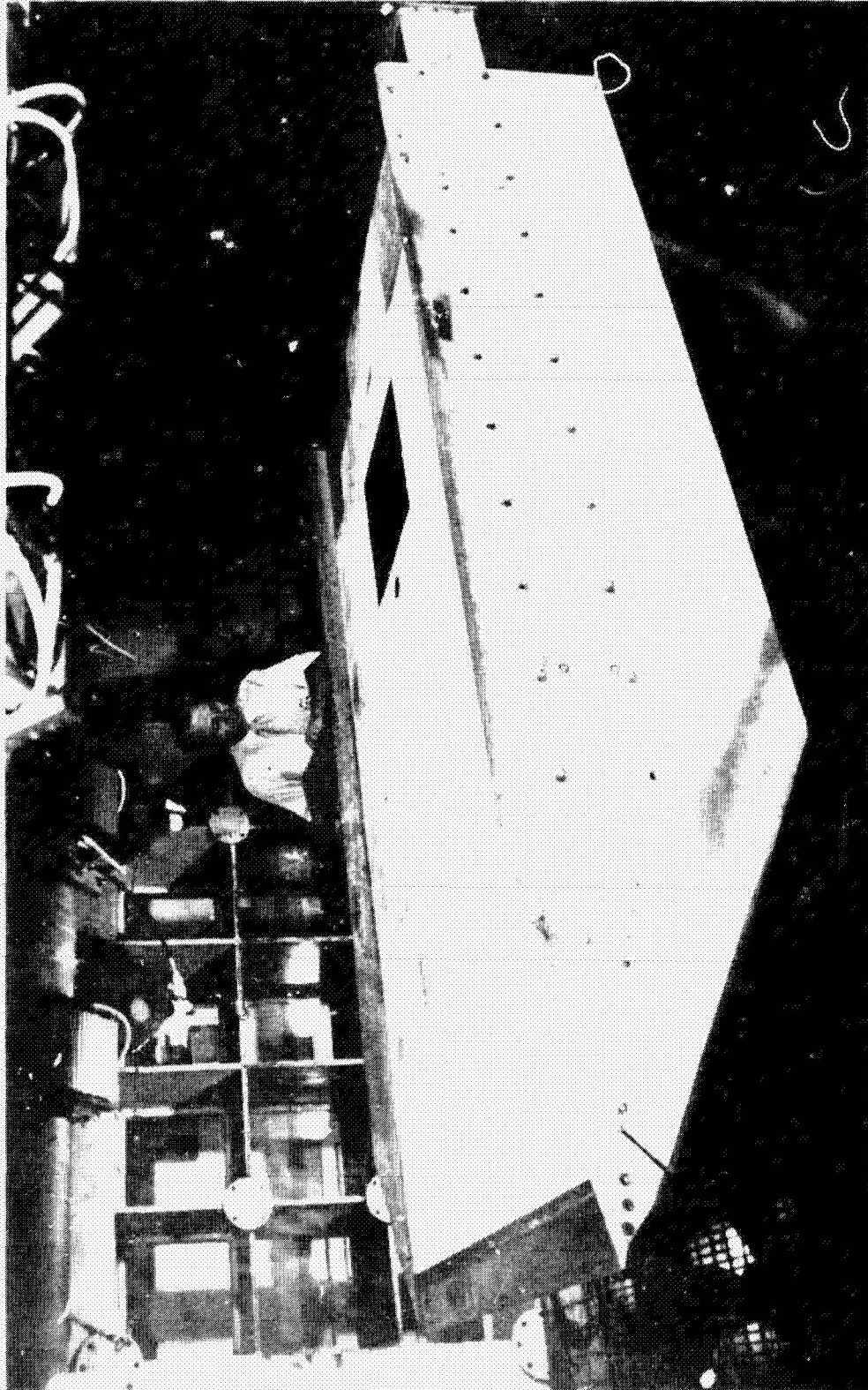
Figure 4.- Photograph of panel holder in Langley 8-foot high-temperature structures tunnel.

L-74-4877
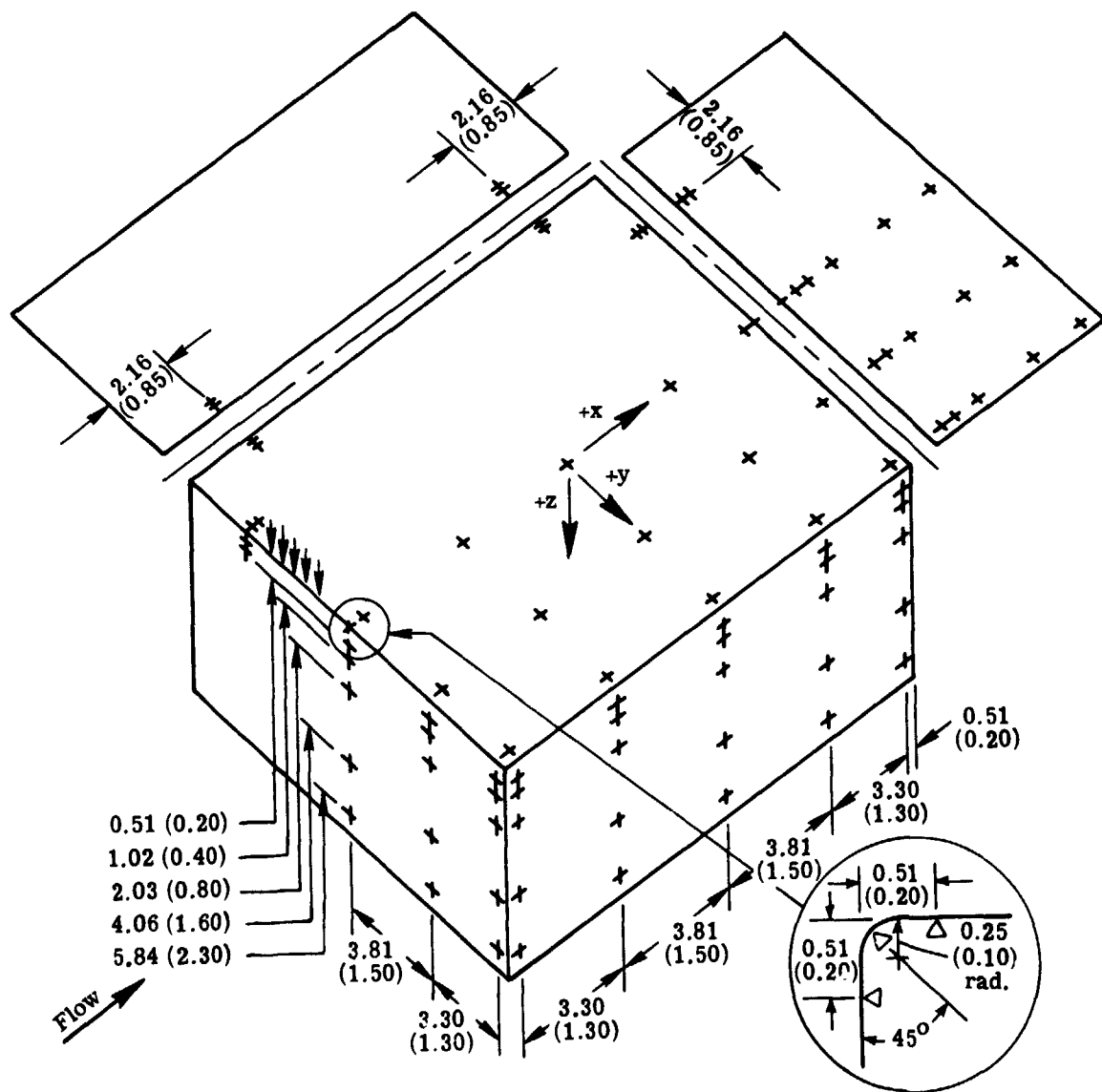
Figure 5.- Nominal thermocouple locations for thin-wall metallic center tile.
Dimensions are in cm (in.).
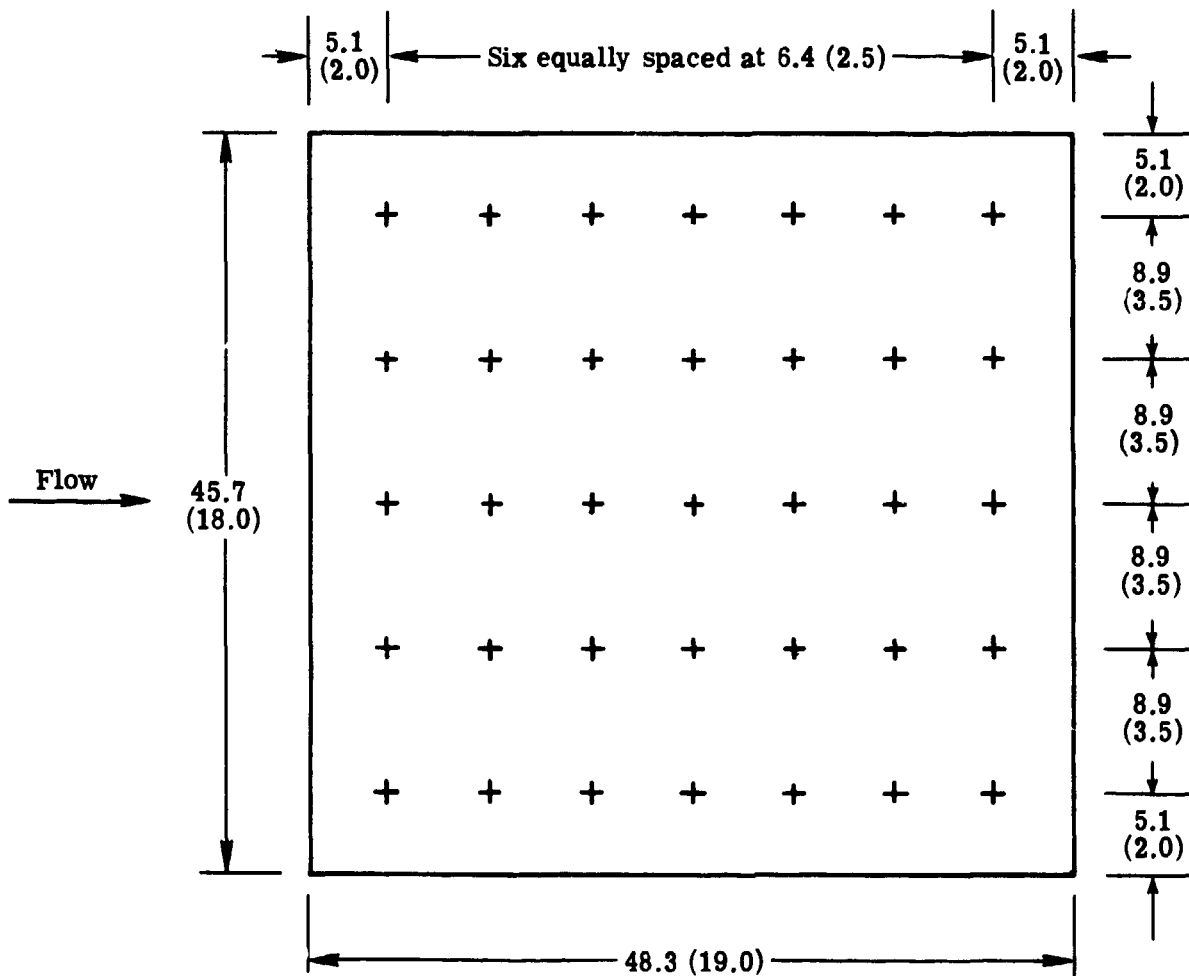
Figure 6.- Thermocouple locations on calibration panel.
Dimensions are in cm (in.).
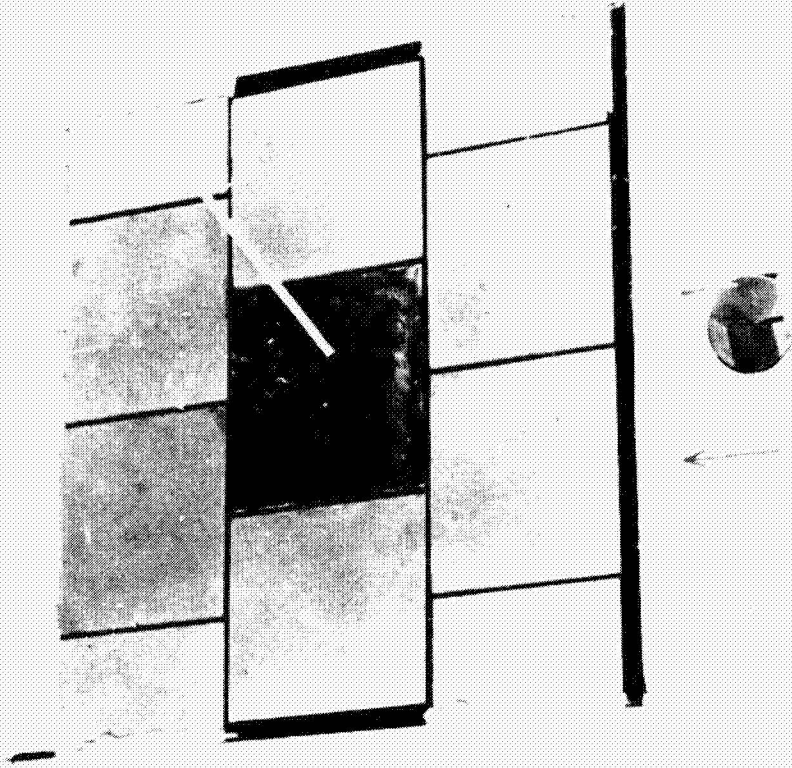
Figure 7.- Tile array mounted in surface of panel holder in staggered tile arrangement.
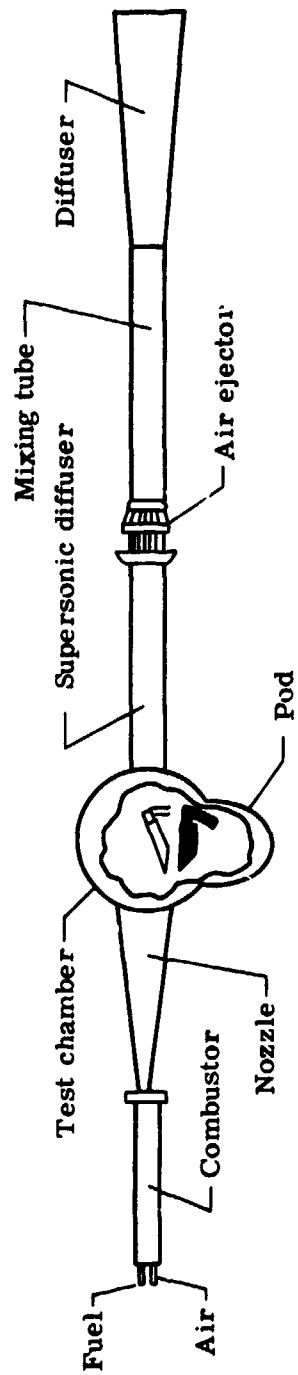
Figure 8.- Schematic drawing of the Langley 8-foot high-temperature structures tunnel.

Fuel

Air

Combustor

Nozzle

Pod

Test chamber

Supersonic diffuser

Mixing tube

Air ejector

Diffuser
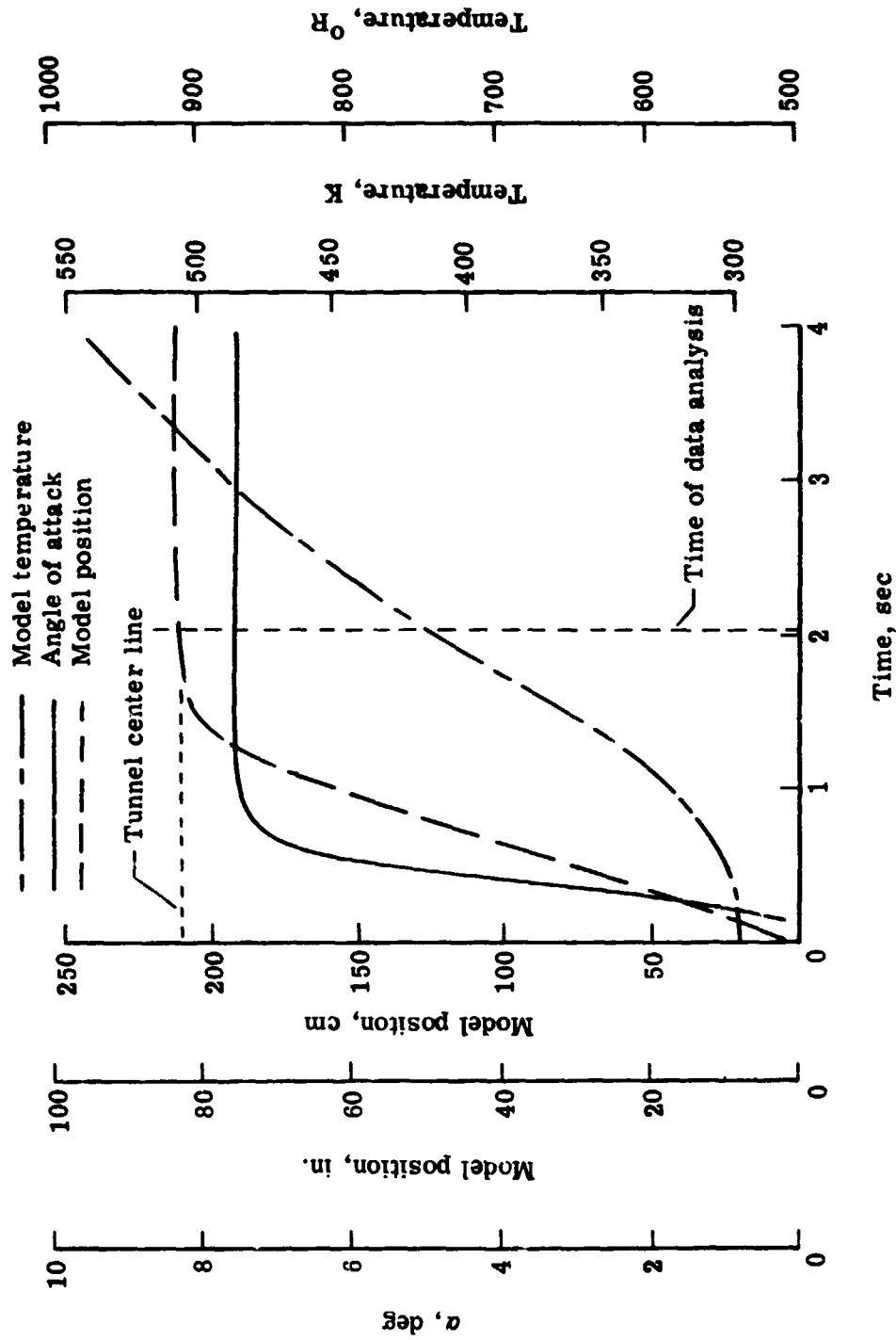
Figure 9.- Typical history of events during model injection into test stream.
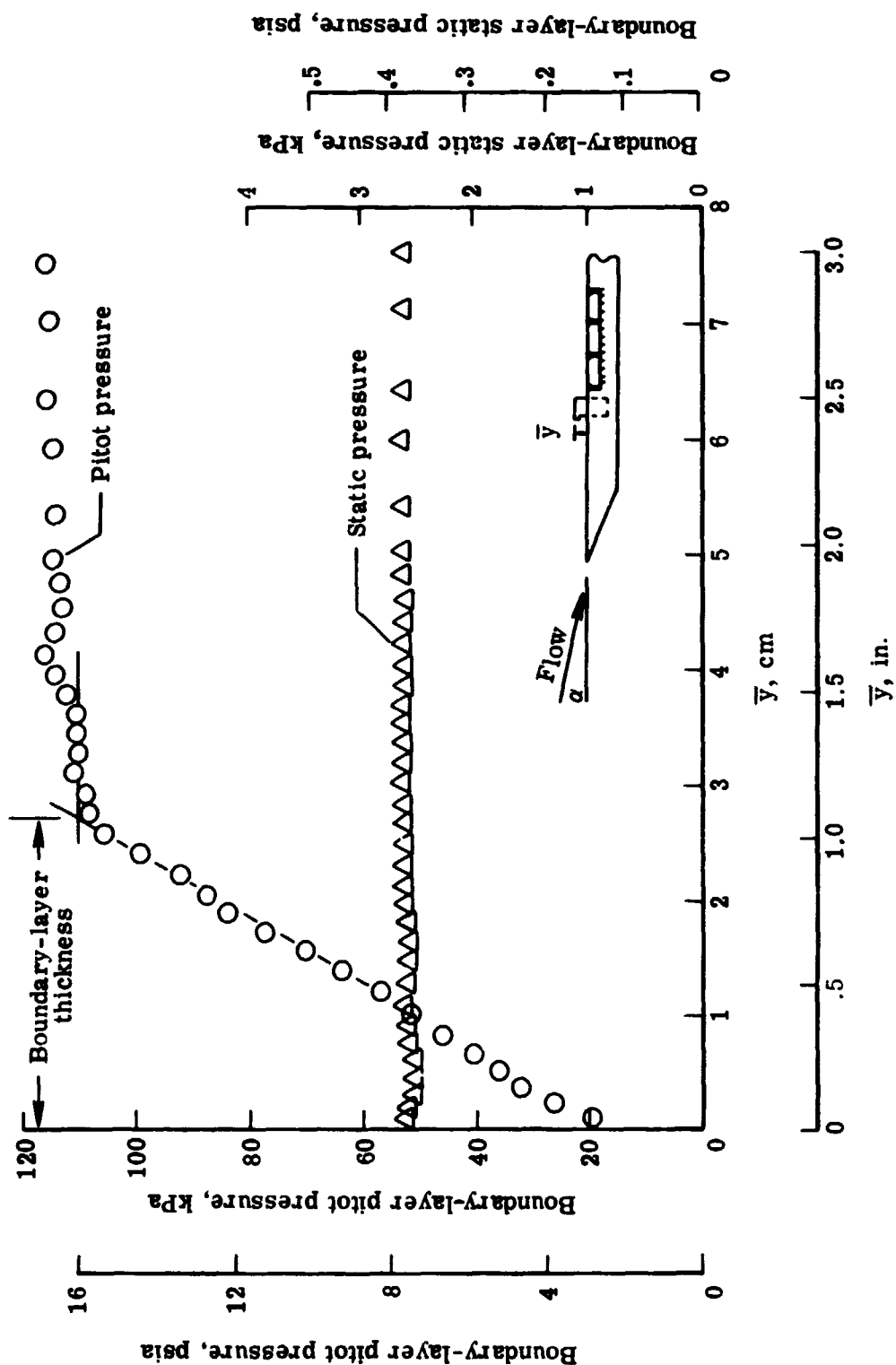
Figure 10.- Boundary-layer pitot and static pressure distributions (run 10).

$$\frac{U}{U_O} = \left(\frac{\bar{y}}{\delta}\right)^{\frac{1}{N}}$$

N = 12.5
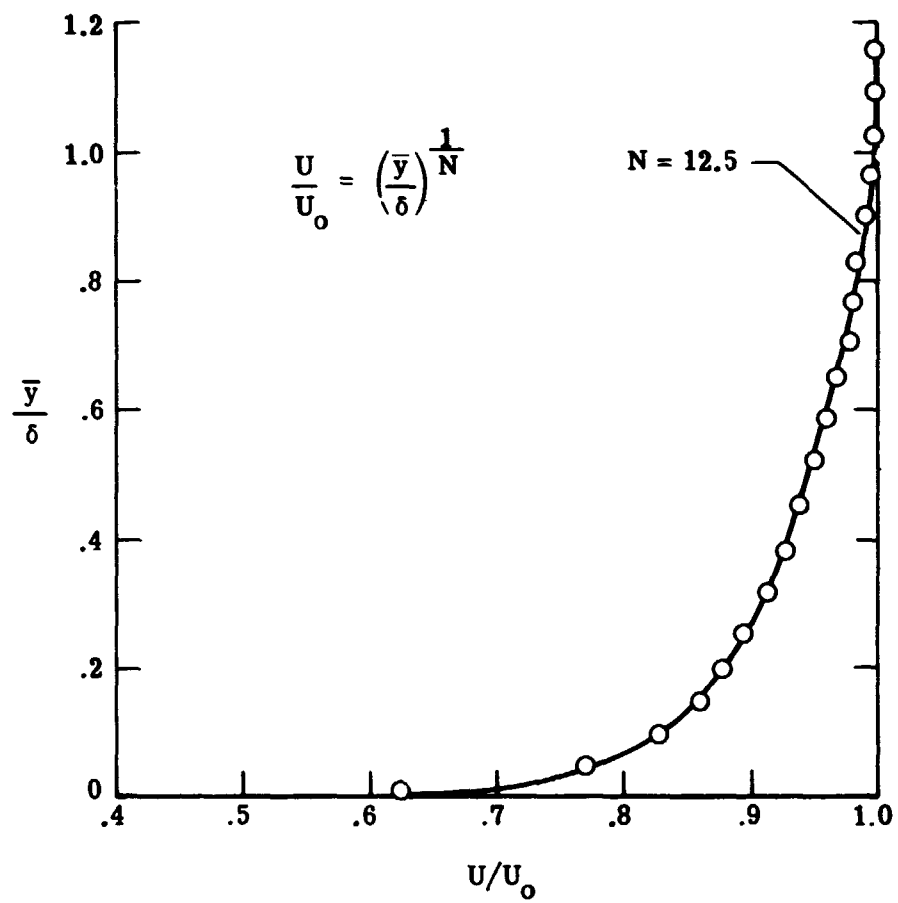
Figure 11.- Power-law curve fit to normalized boundary-layer profile.
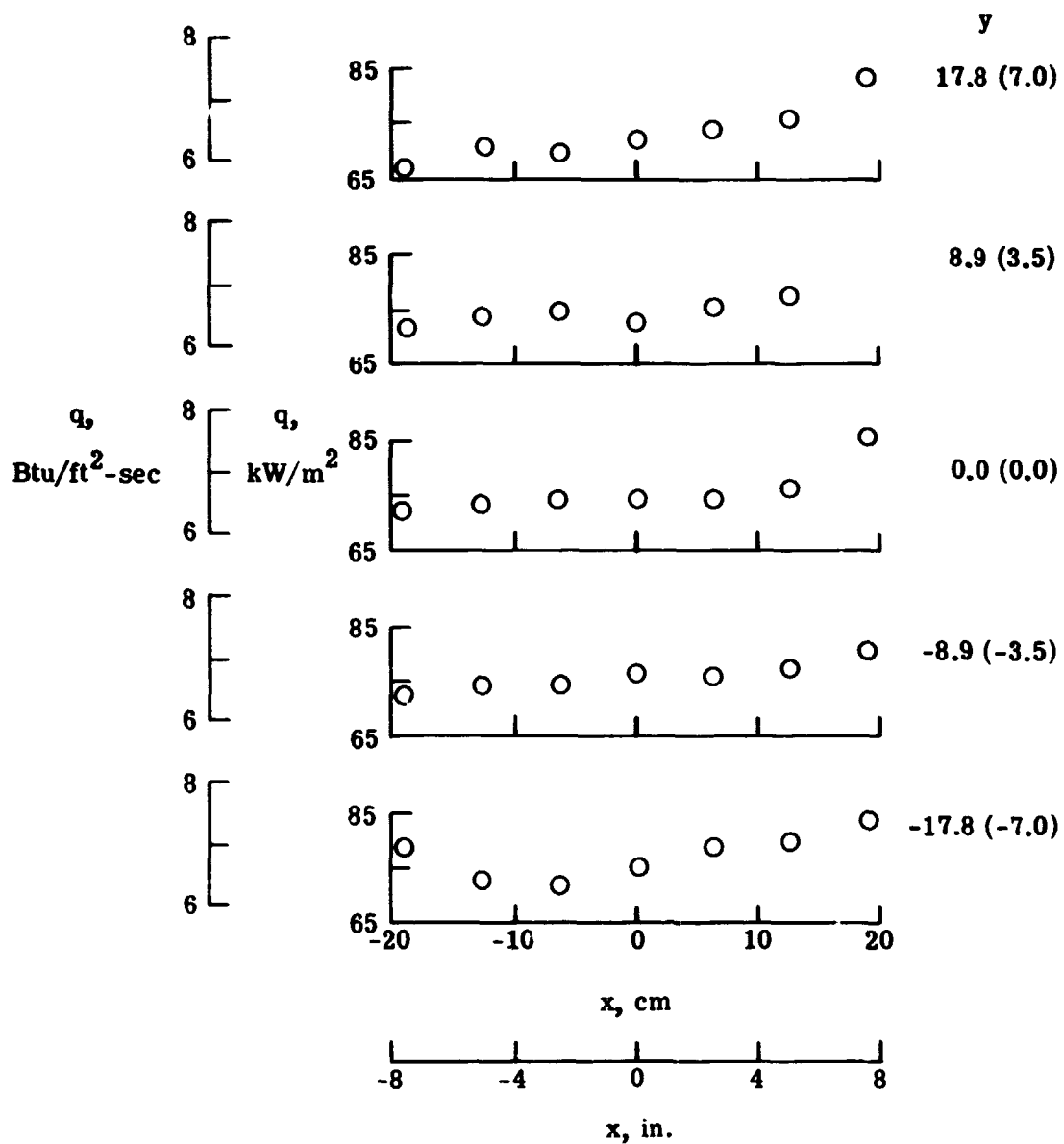
(a) Longitudinal distributions.

Figure 12.- Heating-rate distributions on calibration panel for run 1.
Dimensions are in cm (in.).
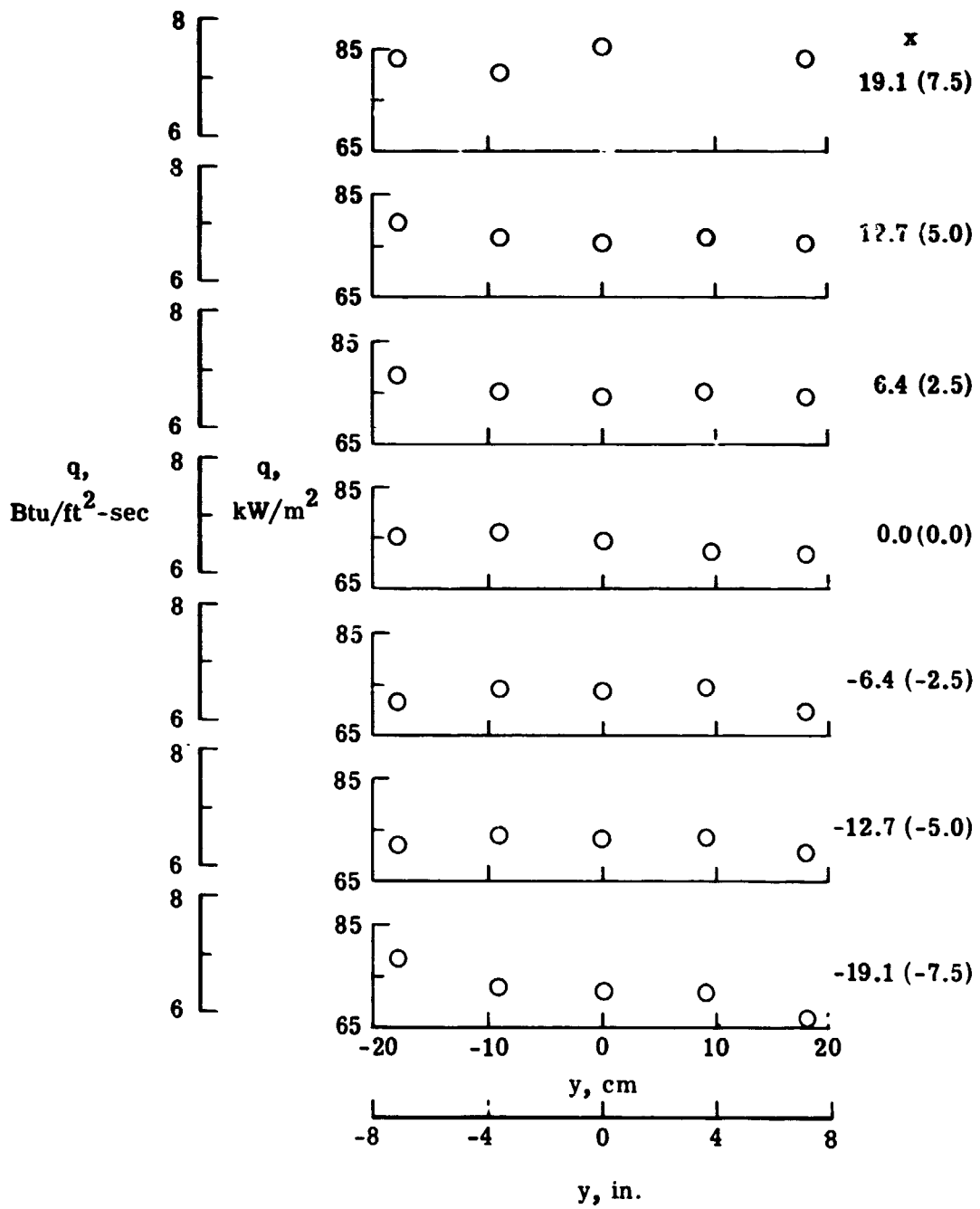
(b) Transverse distributions.

Figure 12.- Concluded.
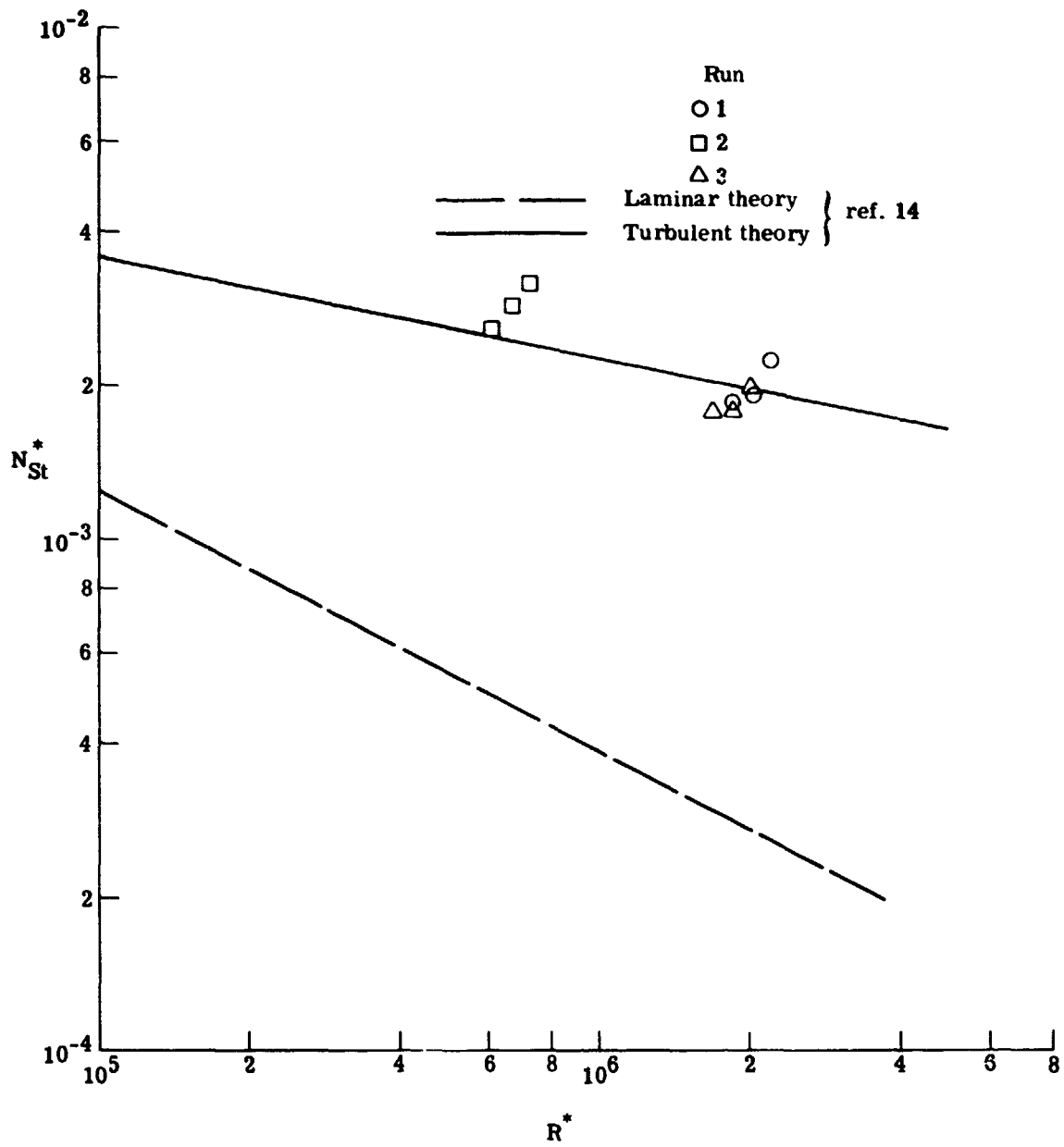
Figure 13.- Heating on calibration panel as a function of local Reynolds number.
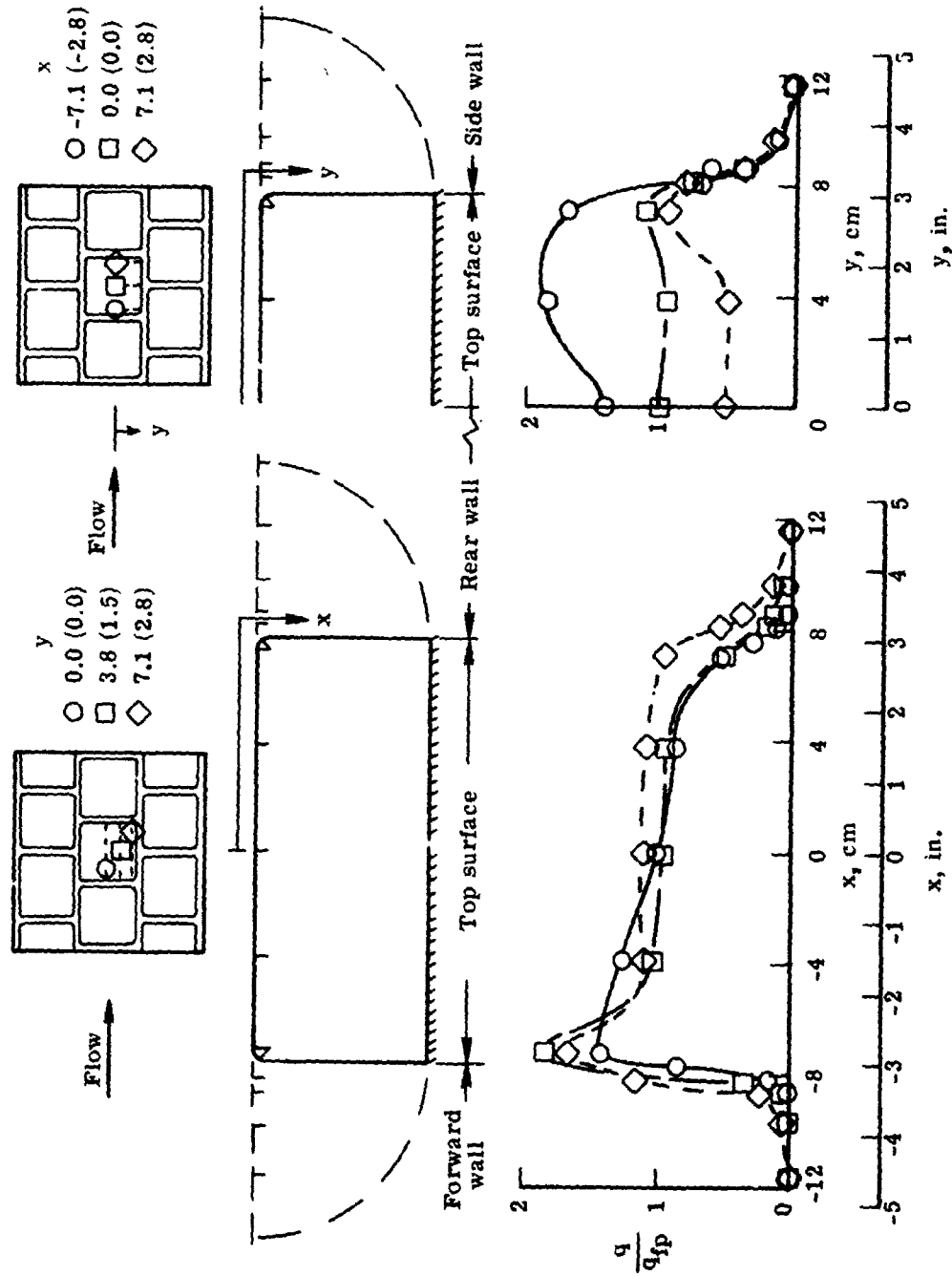
(a) Longitudinal distributions.   (b) Transverse distributions.

Figure 14.- Typical heating-rate distributions for in-line tile arrangement for run 6. $\delta^* = 1.17$ (0.46);

w = 0.18 (0.07).   Dimensions are in cm (in.).
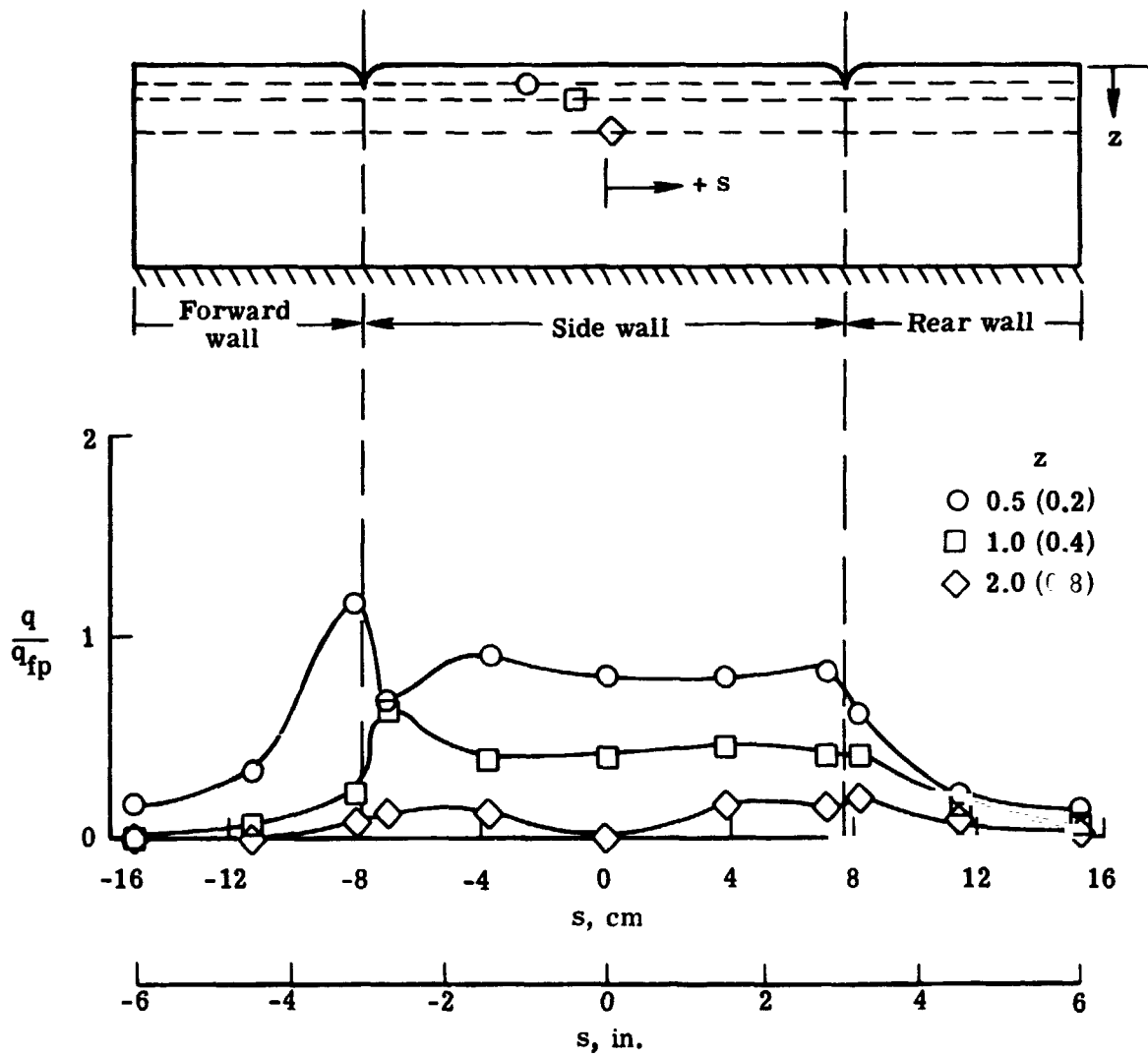
(c) Distributions around tile.

Figure 14.- Concluded.
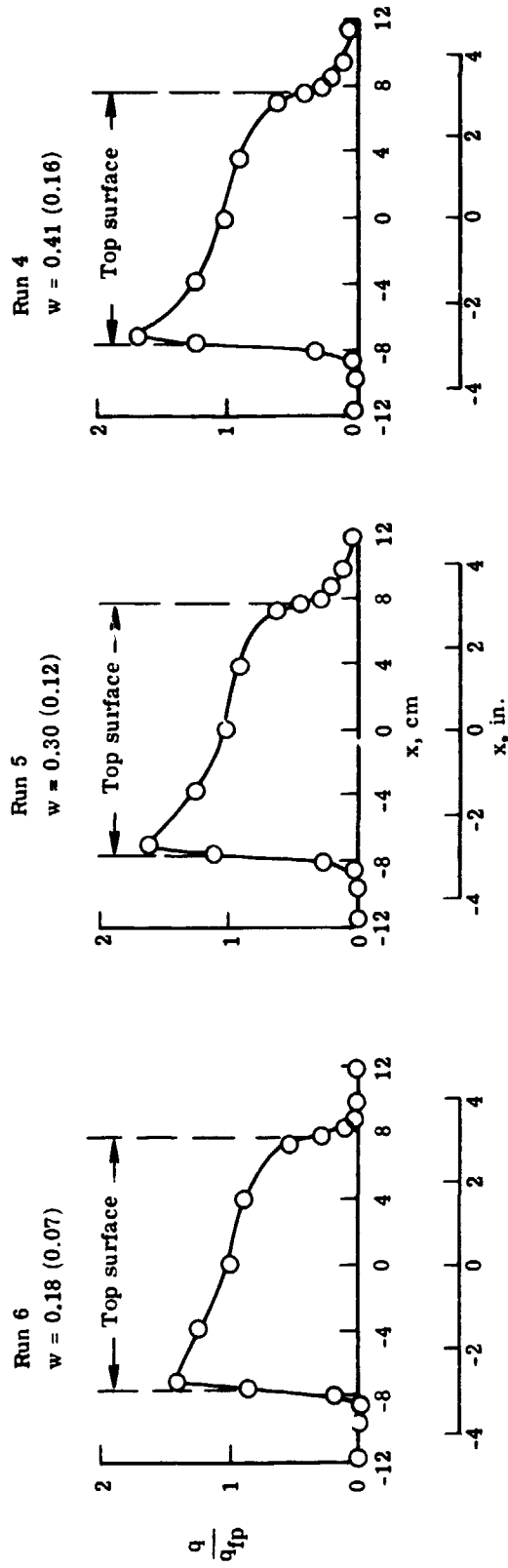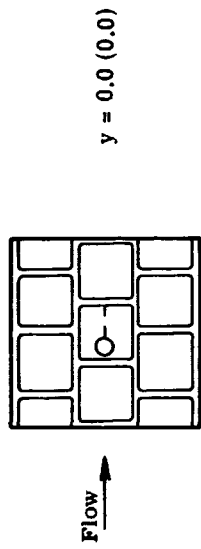
(a) Longitudinal distributions.

Figure 15.- Effect of gap width on heating for in-line tile arrangement, $\delta^* = 1.17$ (0.46). Dimensions are in cm (in.).

34
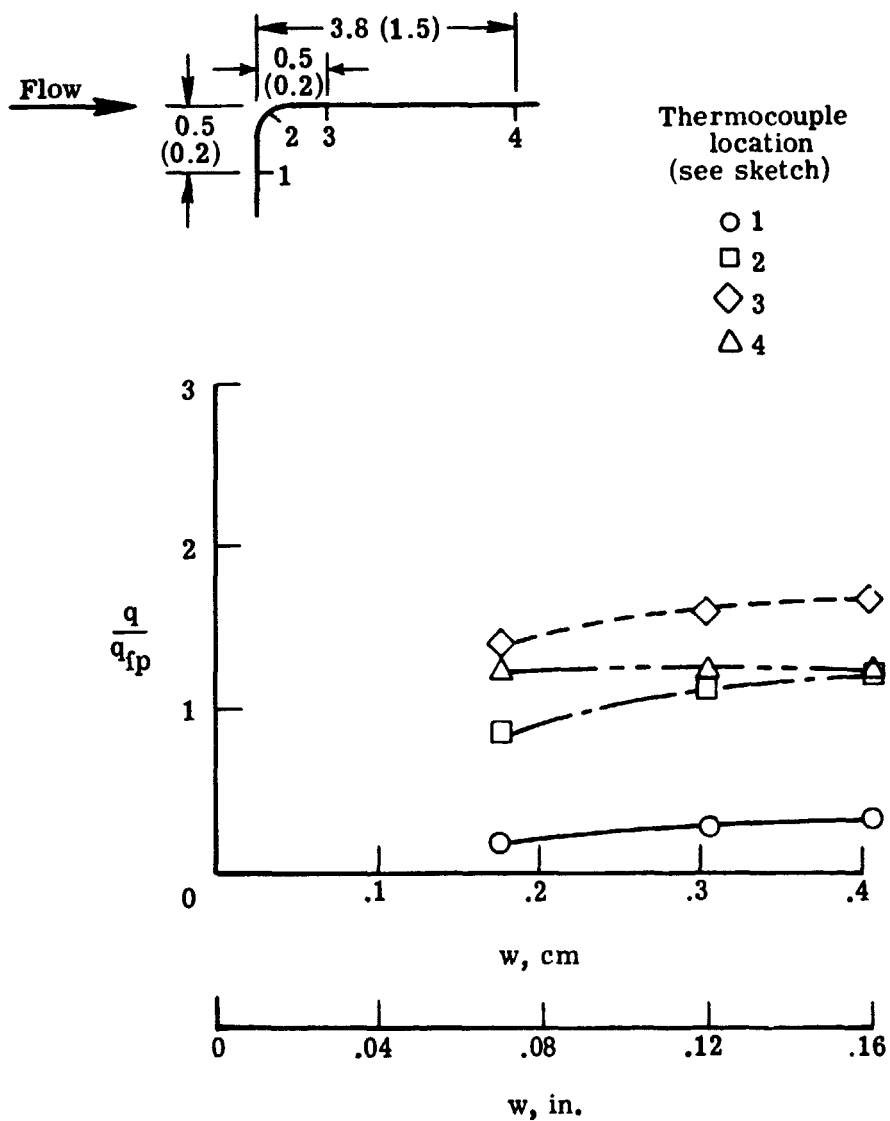
(b) Leading-edge center-line heating.
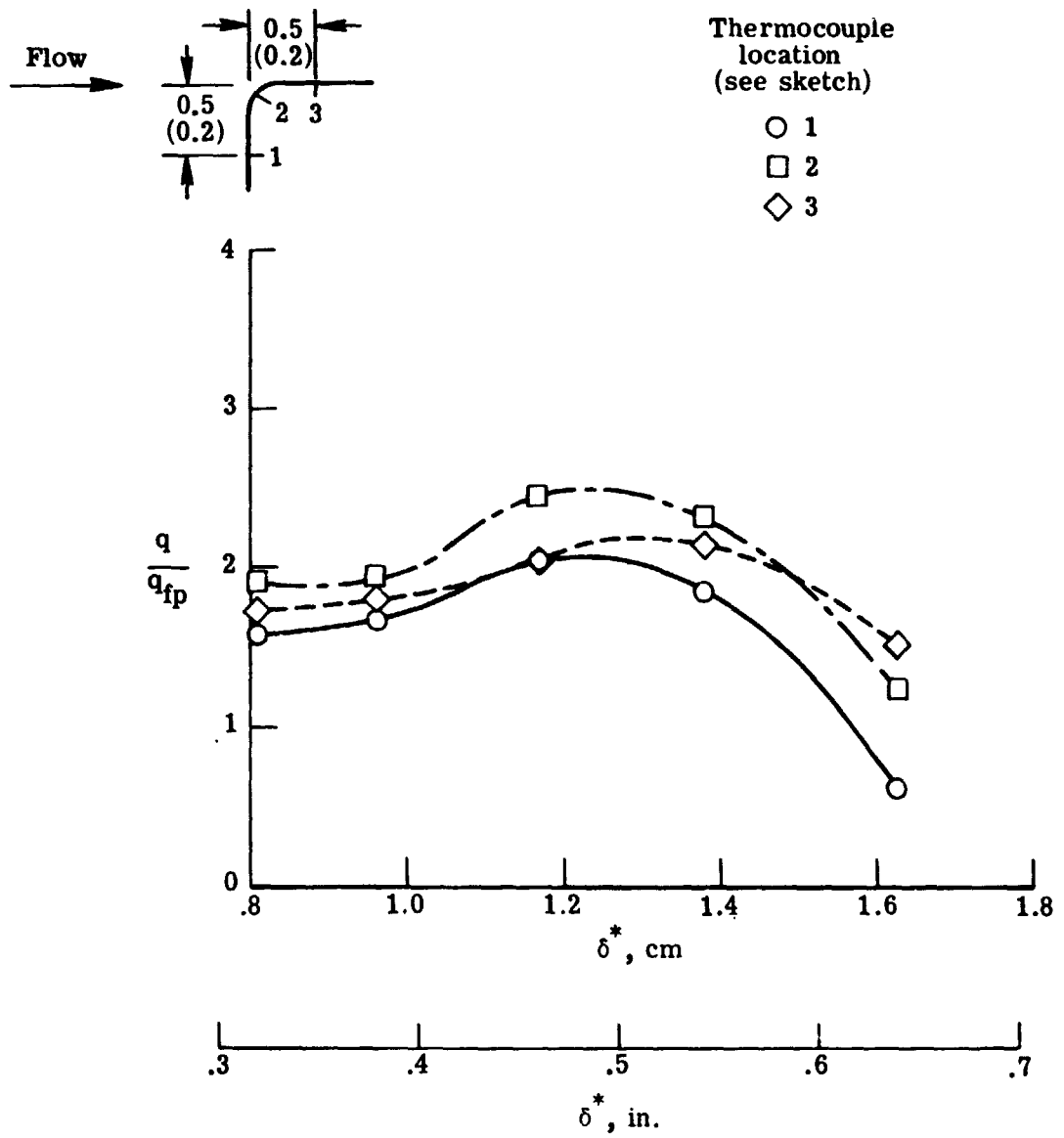
Figure 15.- Continued.
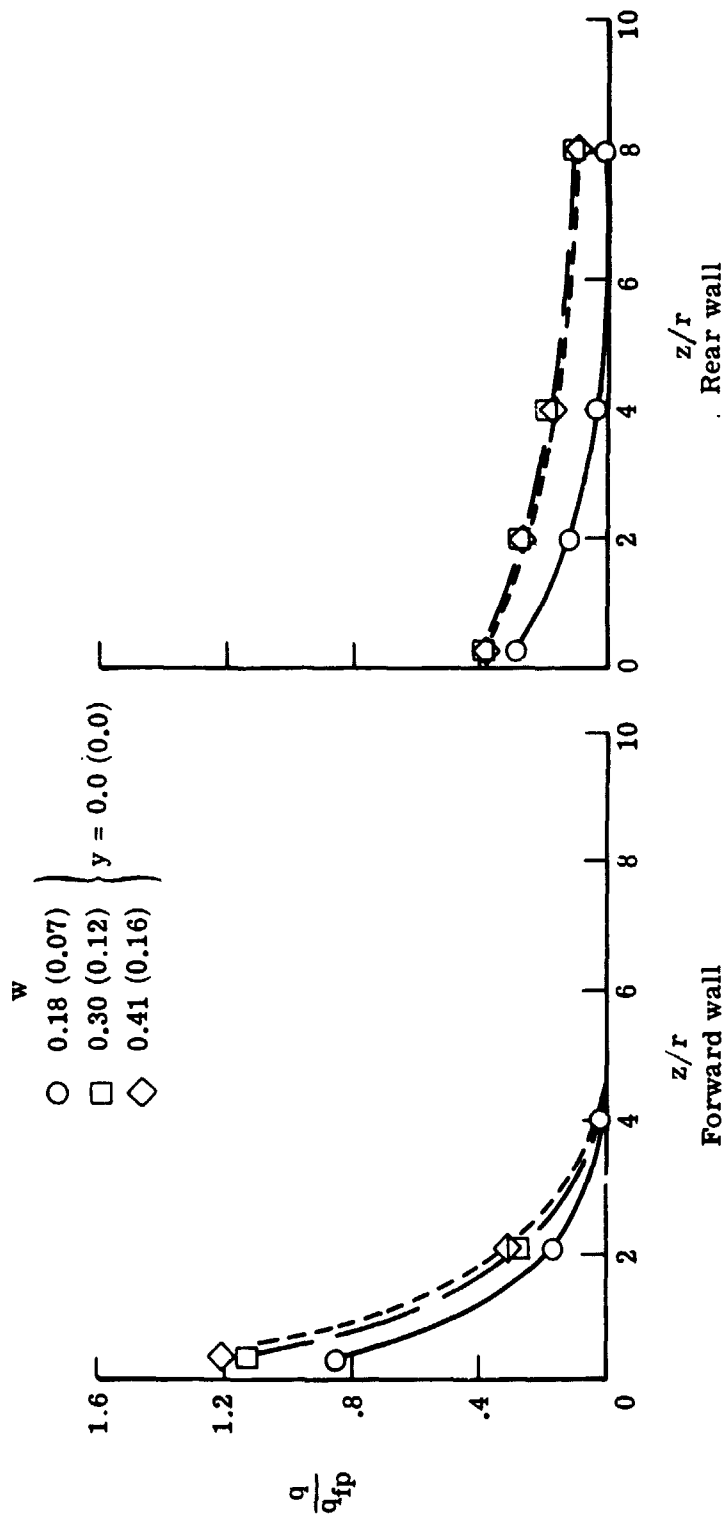
(c) Forward- and rear-wall center-line distributions.

Figure 15.- Concluded.
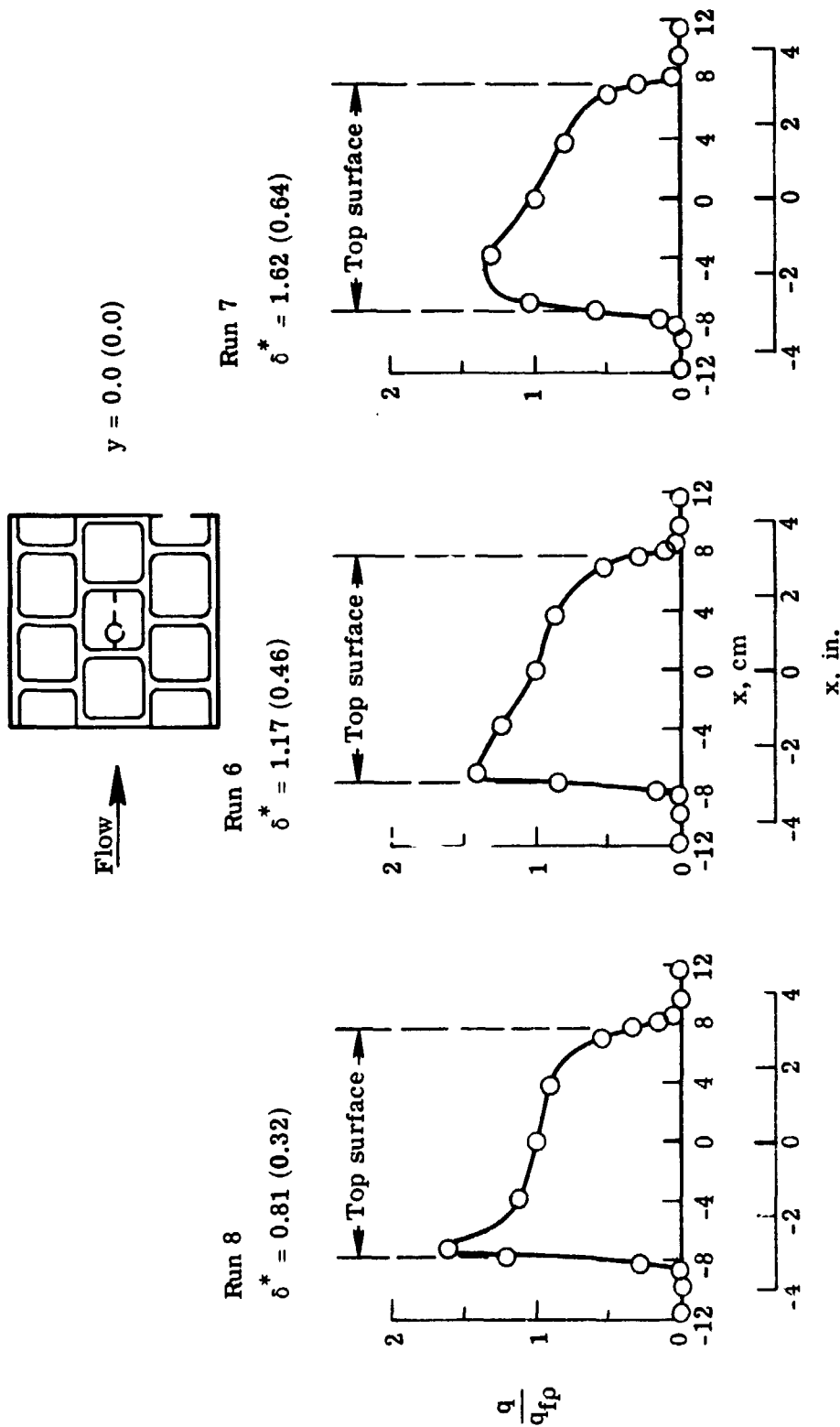
(a) Longitudinal distributions.

Figure 16.- Effect of boundary-layer displacement thickness on heating for in-line tile arrangement, w = 0.18 (0.07). Dimensions are in cm (in.).
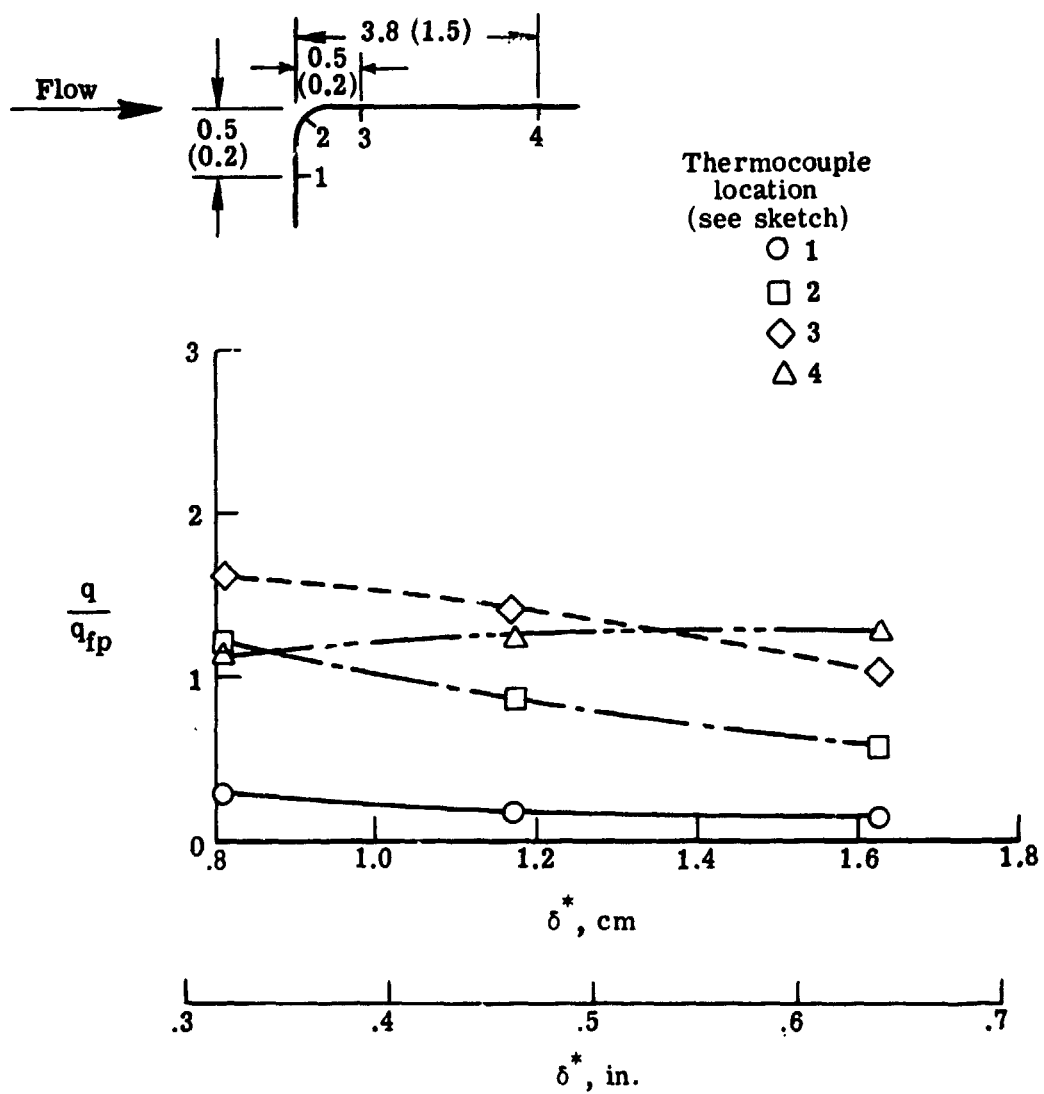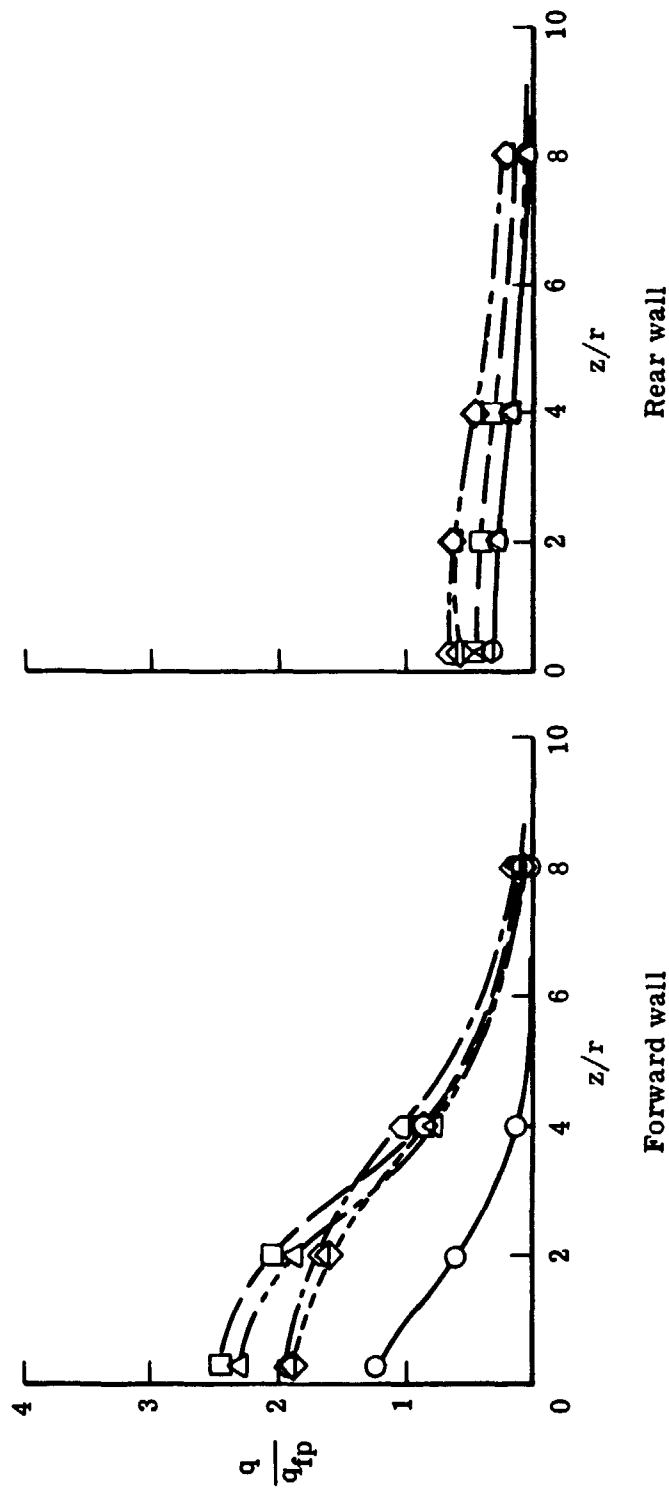
(b) Leading-edge center-line heating.

Figure 16.- Continued.
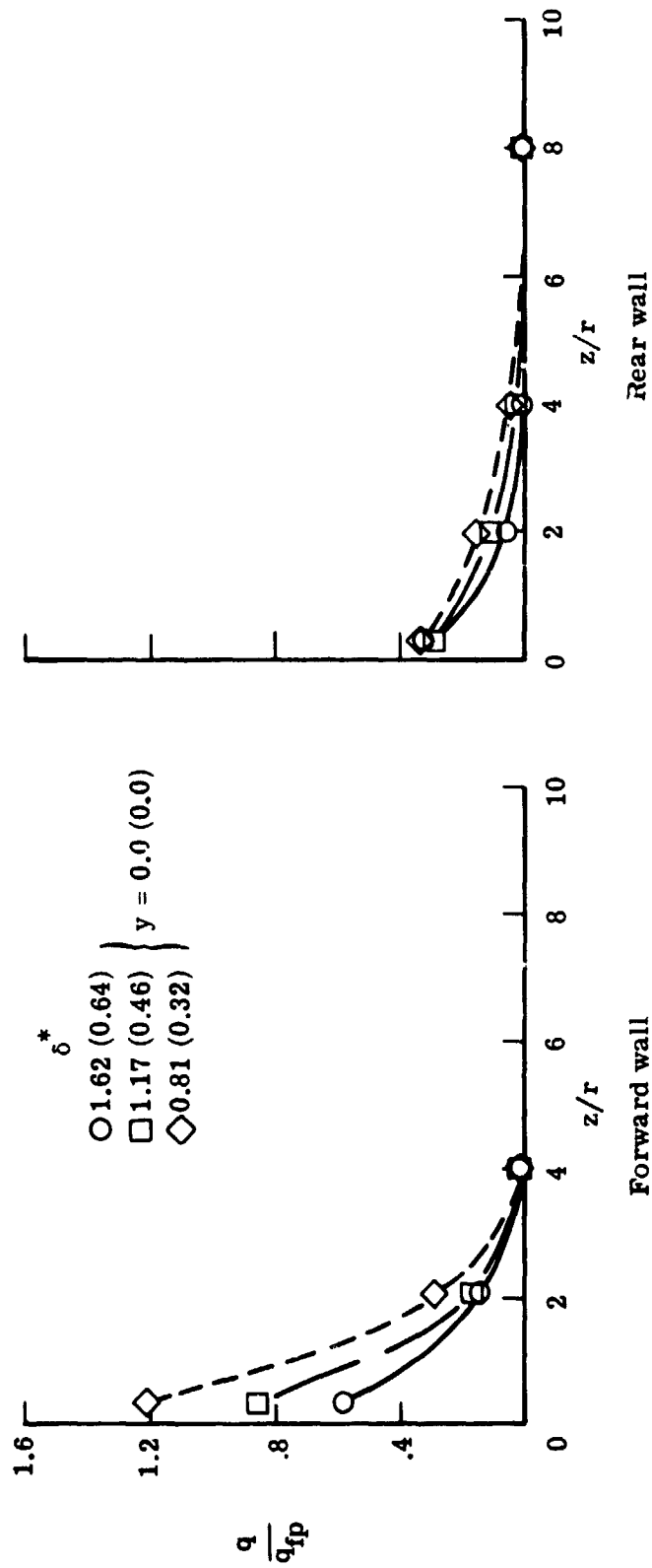
(c) Forward- and rear-wall center-line distributions.

Figure 16.- Concluded

(a) Longitudinal distributions.

(b) Transverse distributions.
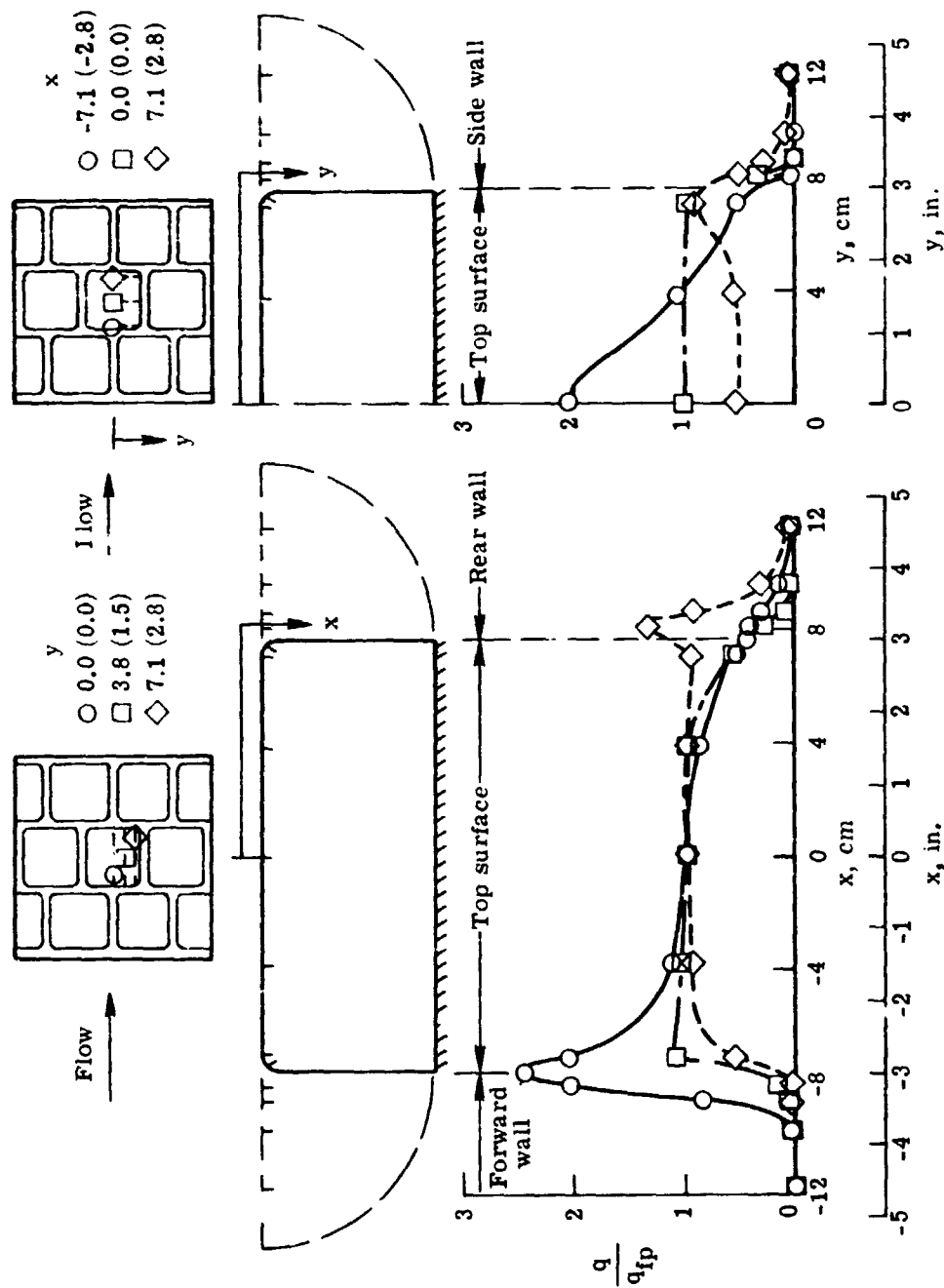
Figure 17.- Typical heating-rate distributions for staggered tile arrangement for run 10. $\delta^* = 1.17$ (0.46); $w = 0.18$ (0.07). Dimensions are in cm (in.).
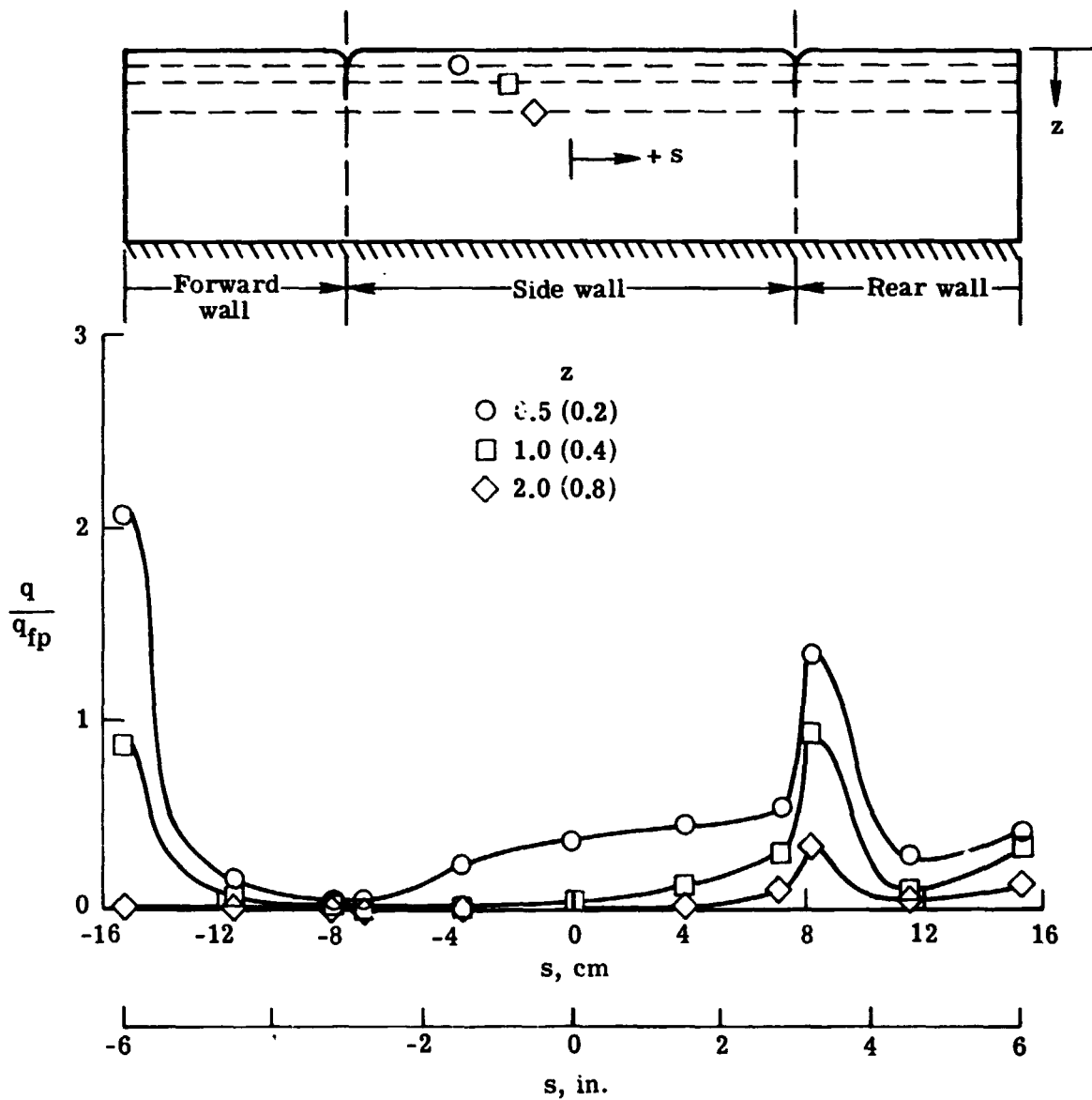
(c) Distributions around tile.

Figure 17.- Concluded.
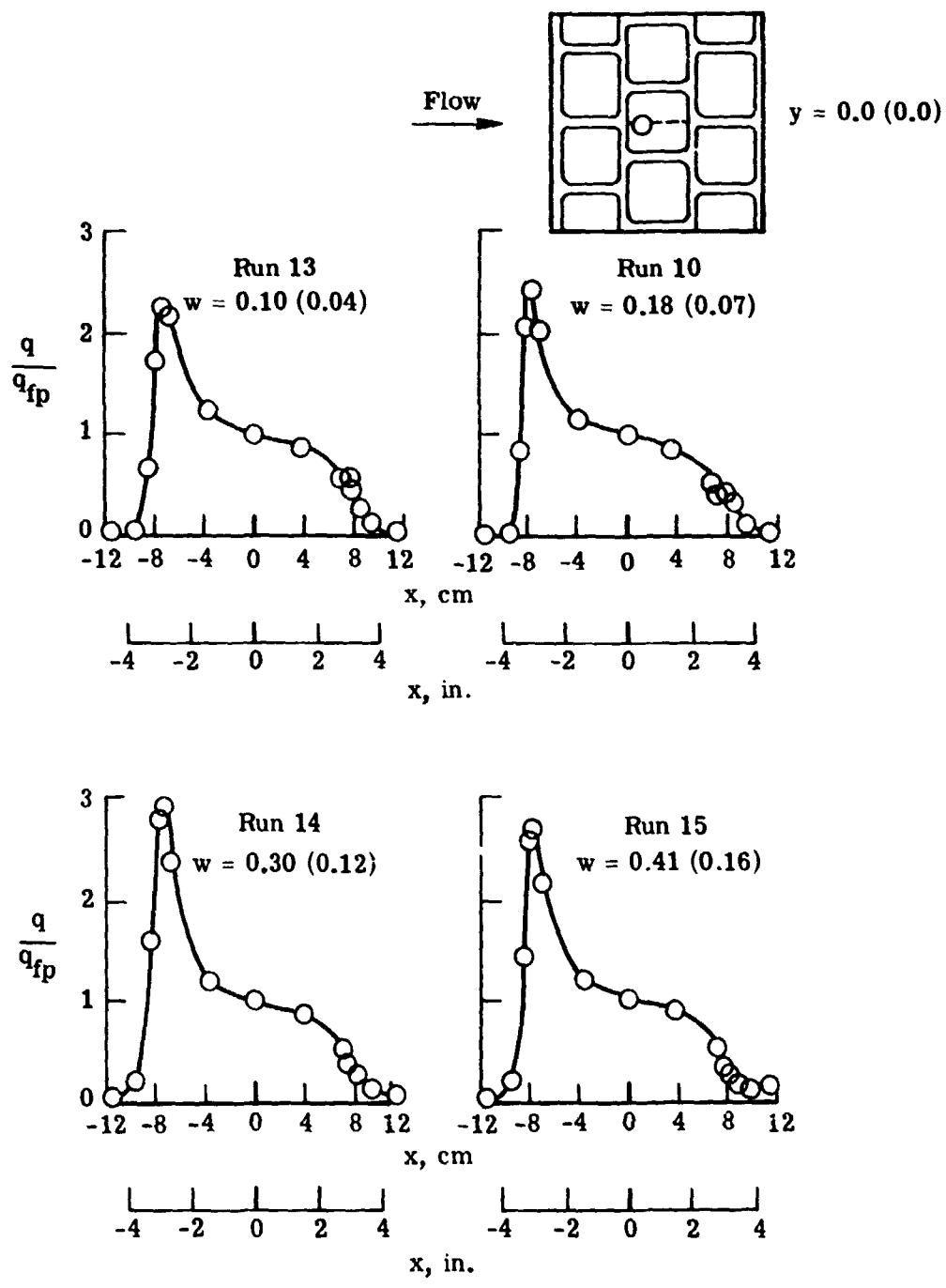
(a) Longitudinal distributions.

Figure 18.- Effect of gap width on heating for staggered tile arrangement.
$\delta^* = 1.17$ (0.46). Dimensions are in cm (in.).
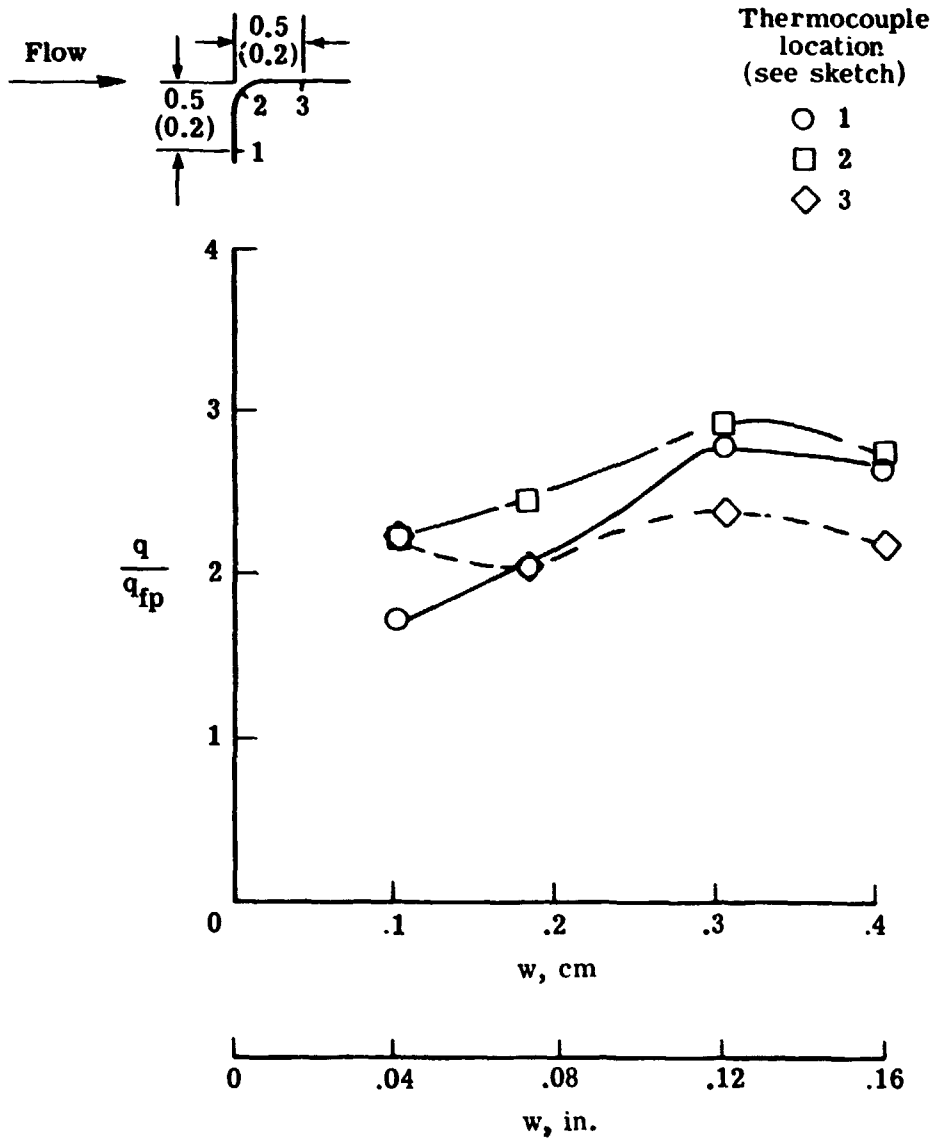
(b) Impingement-region heating.

Figure 18.- Continued.
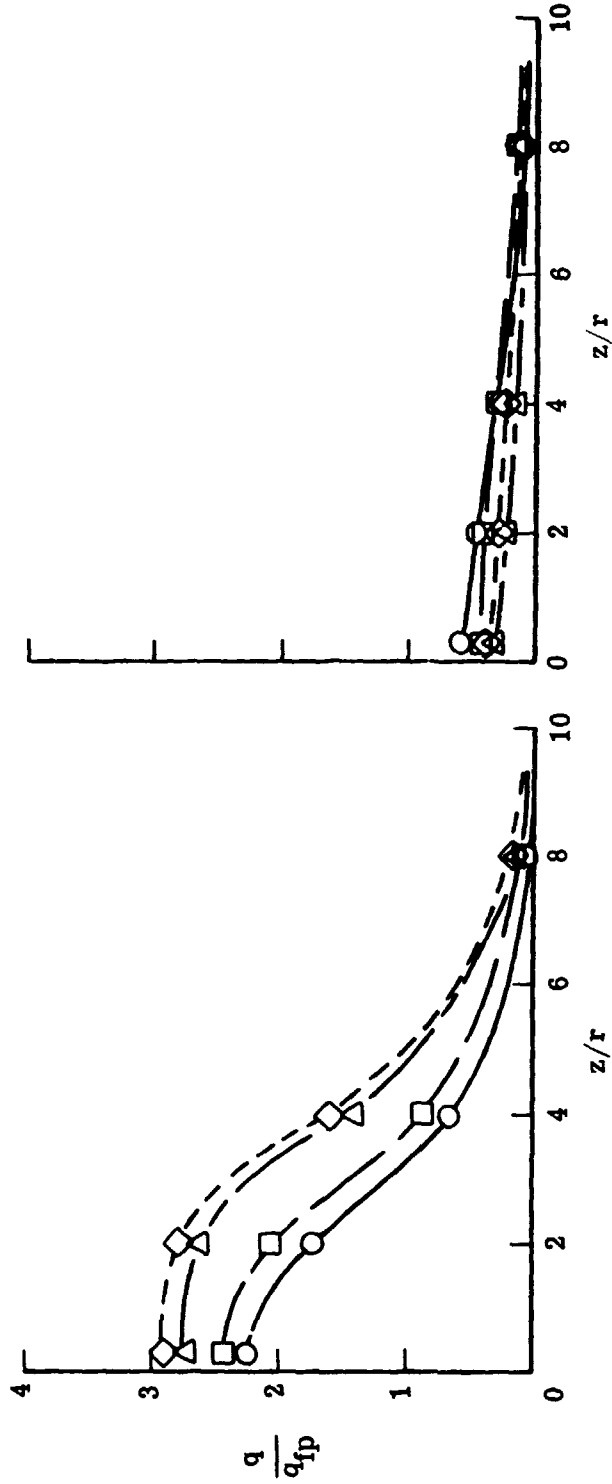
(c) Forward- and rear-wall center-line distributions.

Figure 18.- Concluded.
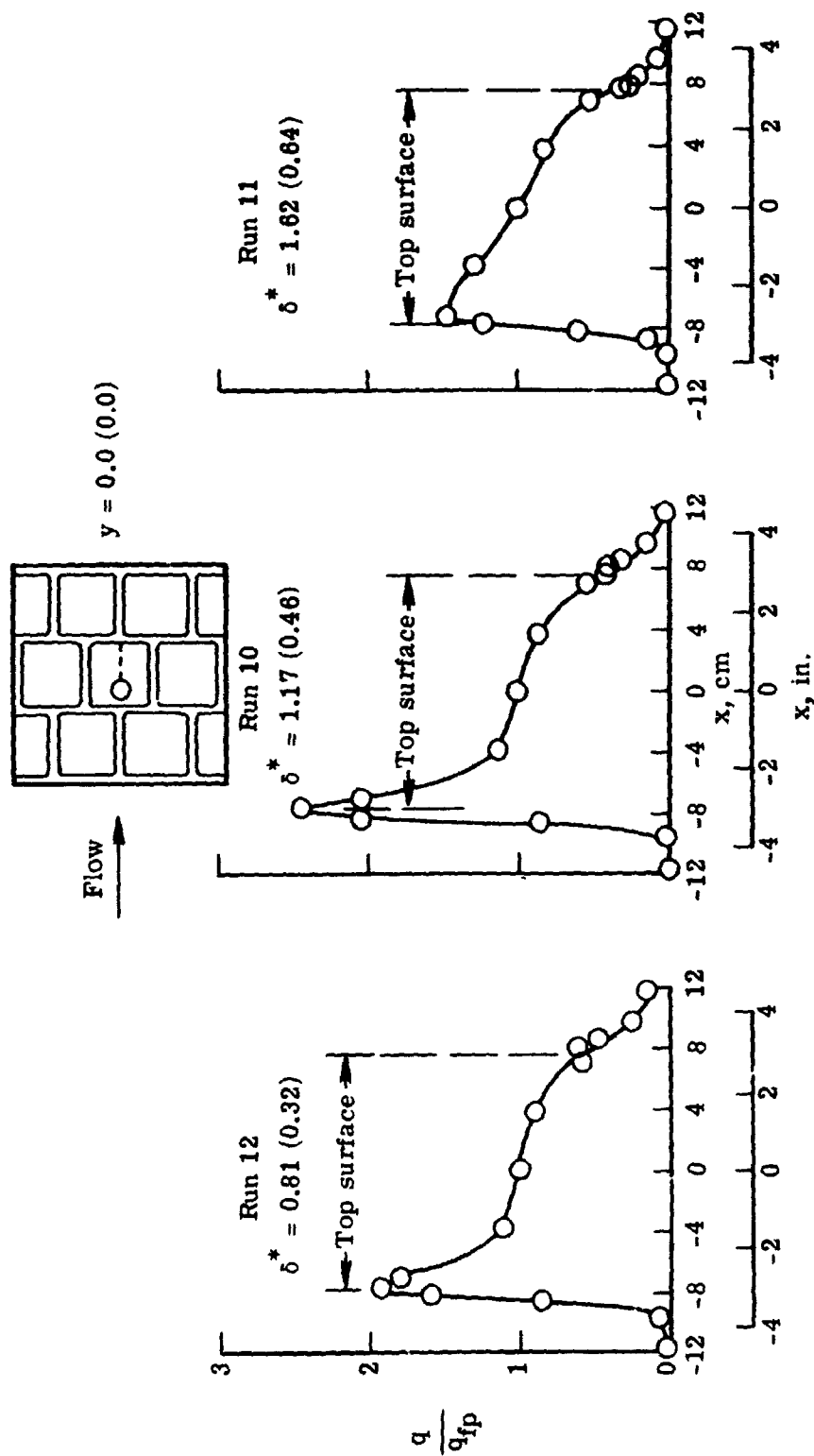
(a) Longitudinal distributions.

Figure 19.- Effect of boundary-layer displacement thickness on heating for staggered tile arrangement. w = 0.18 (0.07). Dimensions are in cm (in.).

(b) Impingement-region heating.

Figure 19.- Continued.

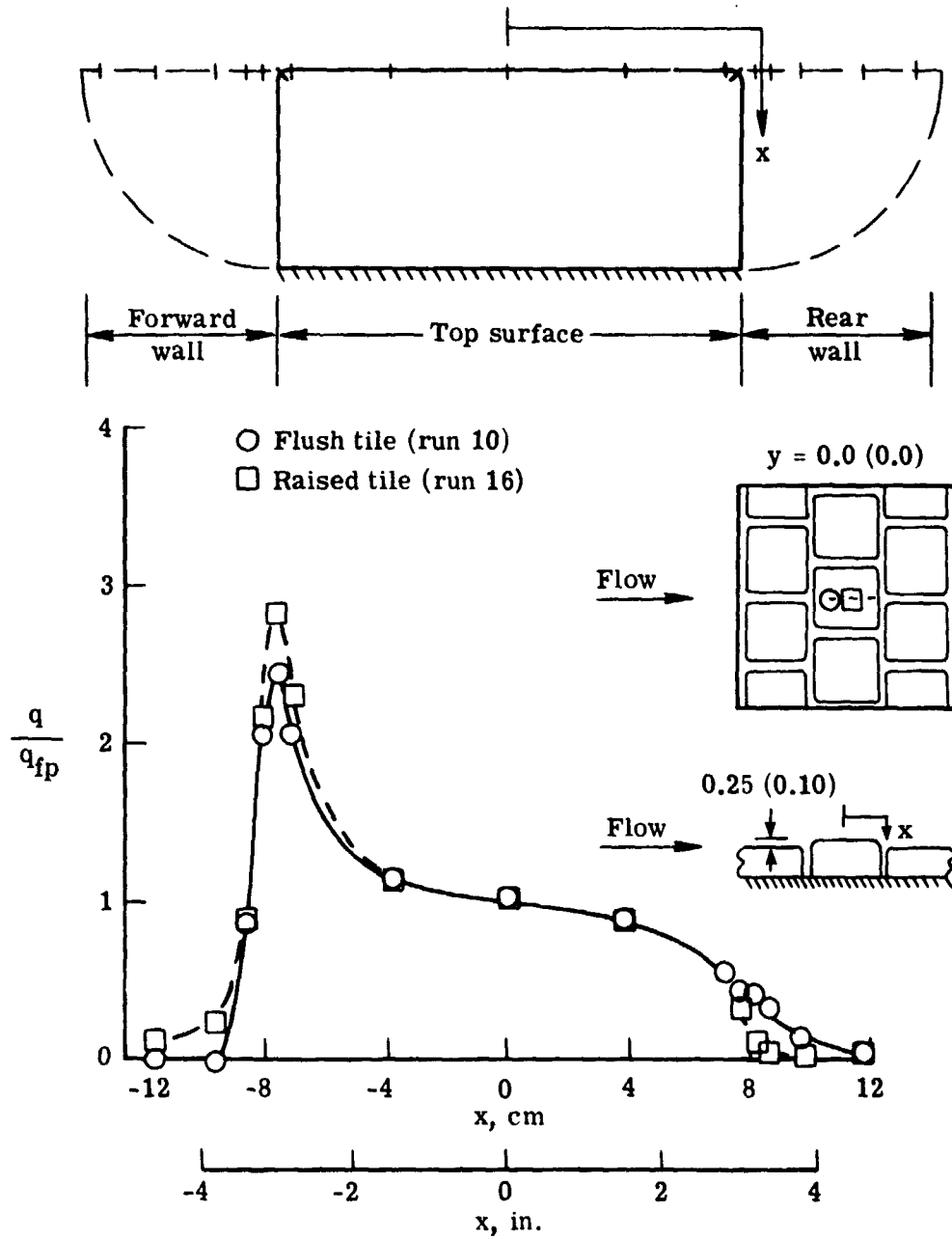(c) Forward- and rear-wall center-line distributions.

Figure 19.- Concluded.
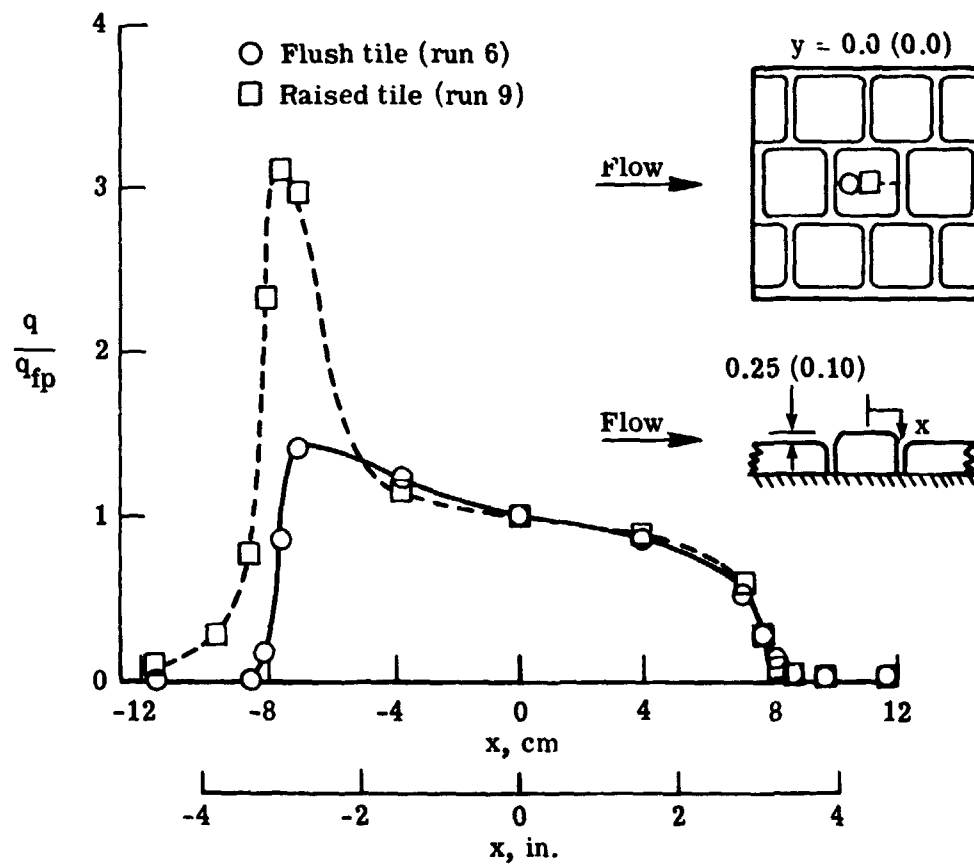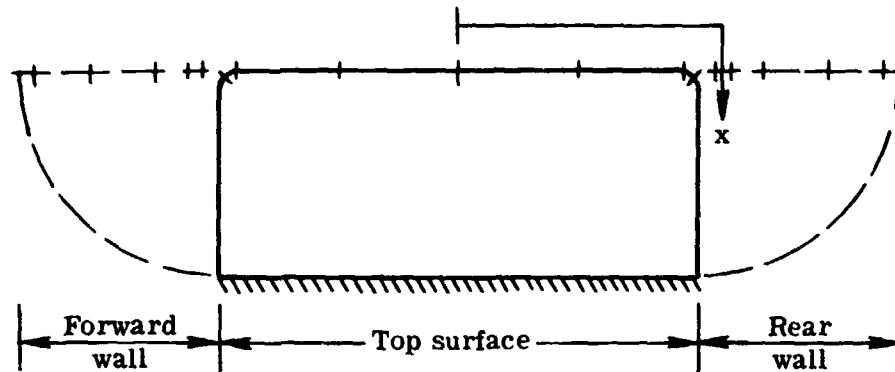
(a) Longitudinal distributions.

Figure 20.- Effect of raised tile on heating for in-line tile arrangement. $\delta^* = 1.17$ (0.46); $w = 0.18$ (0.07). Dimensions are in cm (in.).
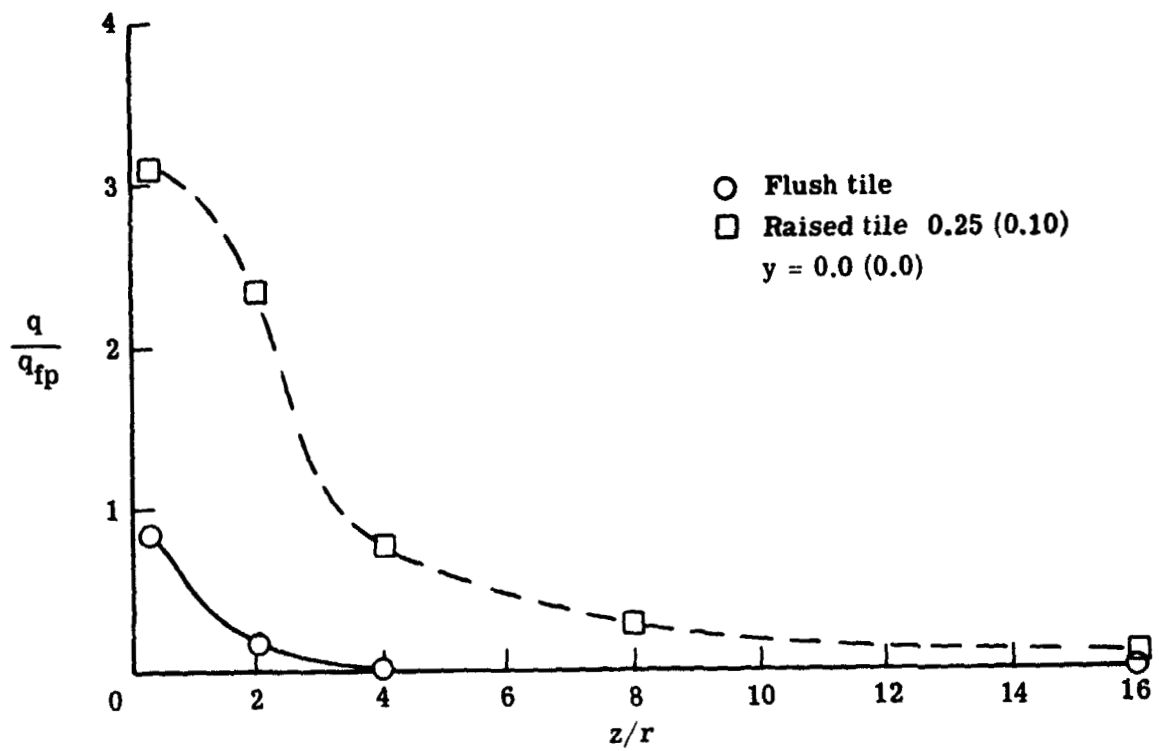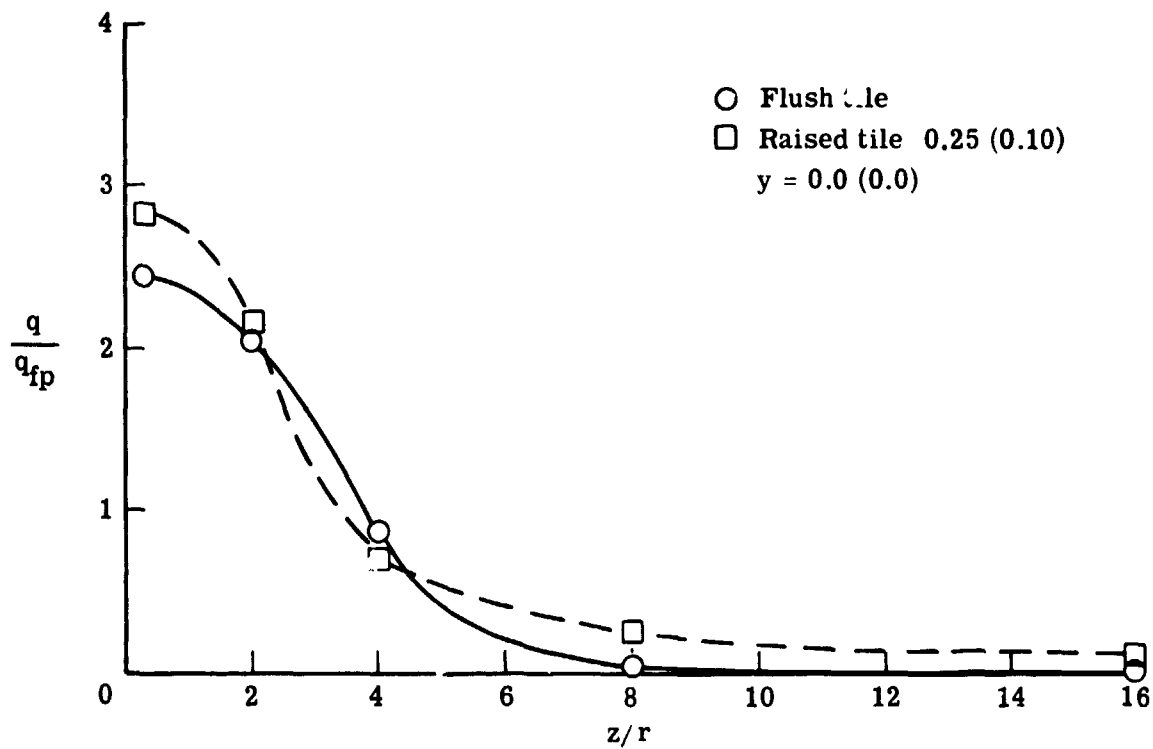
(b) Forward-face center-line distributions.

Figure 20.- Concluded.

(a) Longitudinal distributions.

Figure 21.- Effect of raised tile on heating for staggered tile arrangement. $\delta^* = 1.17$ (0.46); $w = 0.18$ (0.07). Dimensions are in cm (in.).

(b) Forward-face center-line distributions.

Figure 21.- Concluded.